iScience

CellPress

Article

Precise and Cost-Effective Nanopore Sequencing for Post-GWAS Fine-Mapping and Causal Variant Identification

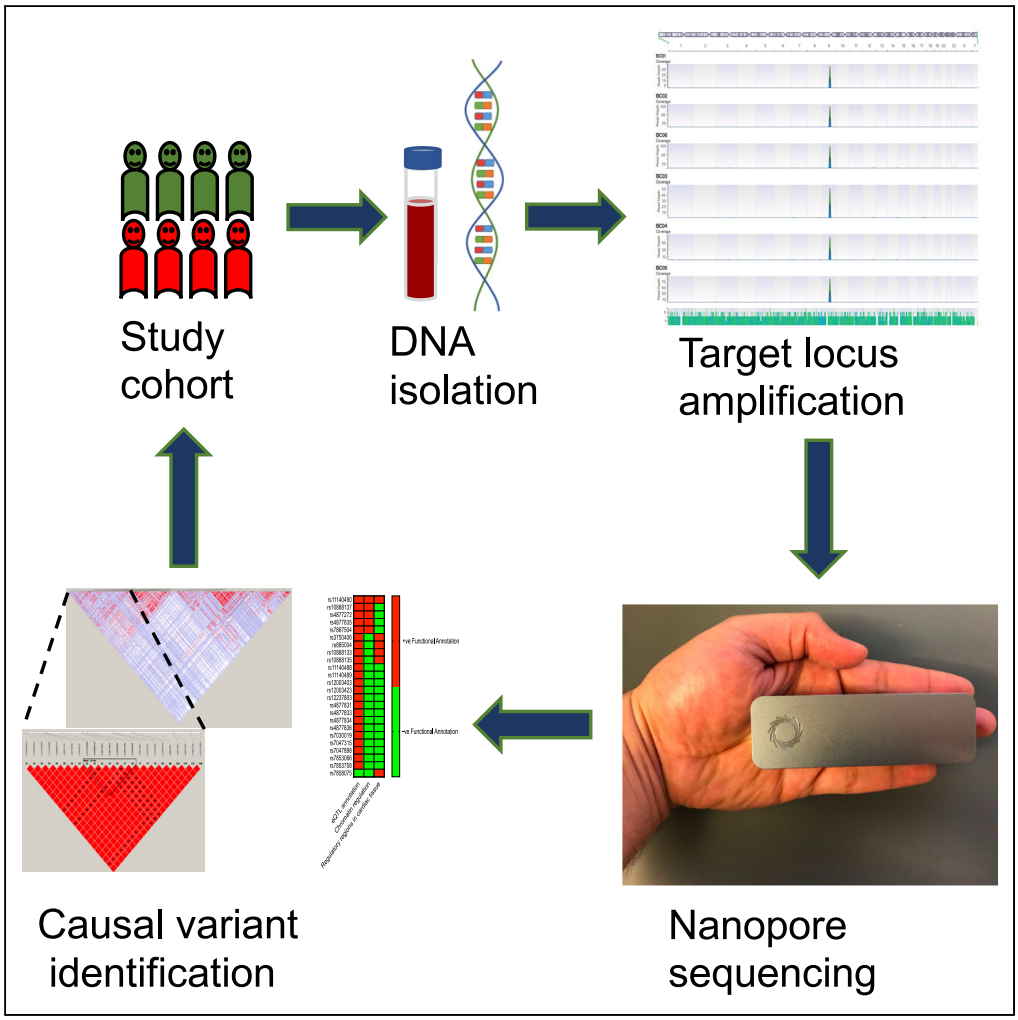

Tarek Magdy, Hui–Hsuan Kuo, Paul W. Burridge

paul.burridge@northwestern.edu

HIGHLIGHTS

Nanopore-based pipeline helps to bridge the gaps between association and causation

This pipeline outperforms imputation in post-GWAS fine-mapping

Helps identify potential causal SNP(s) with a minimal cost of ~$10/100 kb/sample

Magdy et al., iScience *23*, 100971
April 24, 2020
https://doi.org/10.1016/j.isci.2020.100971

iScience

CellPress

Article

Precise and Cost-Effective Nanopore Sequencing for Post-GWAS Fine-Mapping and Causal Variant Identification

Tarek Magdy,[1,2] Hui–Hsuan Kuo,[1,2] and Paul W. Burridge[1,2,3,*]

SUMMARY

Fine-mapping of interesting loci discovered by genome-wide association study (GWAS) is mandatory to pinpoint causal variants. Traditionally, this fine-mapping is completed through increasing the genotyping density at candidate loci, for which imputation is the current standard approach. Although imputation is a useful technique, it has a number of limitations that impede accuracy. In this work, we describe the development of a precise and cost-effective Nanopore sequencing-based pipeline that provides comprehensive and accurate information at candidate loci to identify potential causal single-nucleotide polymorphisms (SNPs). We demonstrate the utility of this technique via the fine-mapping of a GWAS positive hit comprising a synonymous SNP that is associated with doxorubicin-induced cardiotoxicity. In this work, we provide a proof of principle for the application of Nanopore sequencing in post-GWAS fine-mapping and pinpointing of potential causal SNPs with a minimal cost of just ~$10/100 kb/sample.

INTRODUCTION

The genome-wide association study (GWAS) is one of the most commonly used pharmacogenomic approaches and provides positive statistical associations between variants and an investigated phenotype (Magdy and Burridge, 2018). The vast majority of GWASs depend solely on genotyping chips that capture only hundreds of thousands of SNPs known as "tag SNPs" that are distributed across the entire genome (MacArthur et al., 2017). Tag SNPs are SNPs in perfect linkage disequilibrium (LD) with many other neighboring SNPs and act as surrogates for their detection. Thus, a statistically significant GWAS hit is always co-inherited (linked) with several other SNPs that have indistinguishable statistical associations with the studied phenotype, leaving us with numerous possibilities to investigate in relation to causality. Owing to this LD issue, GWASs require downstream fine-mapping and further genetic examination at candidate loci to provide more comprehensive information about positive hits and eventually narrow down the list of potential causal SNPs for downstream mechanistic validation (Magdy et al., 2016).

Importantly, traditional fine-mapping essentially starts with identifying all variants that are co-inherited with a GWAS statistically significant association through increasing the genotyping density at candidate loci, for which imputation is the current standard approach. Imputation infers information about un-typed markers by comparing a genotyped cohort with a population-specific reference panel of haplotypes. HapMap3 (Altshuler et al., 2010) and 1,000 genomes phase 3 (Genomes Project et al., 2010; Abecasis et al., 2012) reference panels are frequently used in imputation comprising 1.6 M and ~80 M genotyped SNPs in 1,184 and 2,504 individuals across different ancestor populations, respectively. Although imputation algorithms have added more power to GWASs, imputed genotypes accuracy is influenced by several factors. Although pre-phasing of the target dataset increases imputation speed, it decreases imputation accuracy as compared with no pre-phasing (Roshyara et al., 2016). Imputation at chromosome X (apart from pseudo autosomal regions) for which males are haploid requires special care, as this hemizygosity reduces effective population size (N_e), resulting in misleading longer shared haplotype stretches between individuals, and thus affects imputation accuracy (Konig et al., 2014). Imputation accuracy is also inversely correlated with lower minor allele frequency making it more challenging to predict rare alleles (Marchini and Howie, 2010). Selecting the correct reference panel is very critical for imputation accuracy; thus, mixed ethnicities heterogeneous cohorts could affect predicted genotypes (Browning, 2008). Different genotyping chips, study sample size, number of missed genotypes, and different imputation software could affect the accuracy of imputed genotypes (Marchini and Howie, 2010). Finally, imputation could provide

[1]Department of Pharmacology, Northwestern University Feinberg School of Medicine, Chicago, IL 60611, USA

[2]Center for Pharmacogenomics, Northwestern University Feinberg School of Medicine, Chicago, IL 60611, USA

[3]Lead Contact

*Correspondence: paul.burridge@northwestern.edu

https://doi.org/10.1016/j.isci.2020.100971

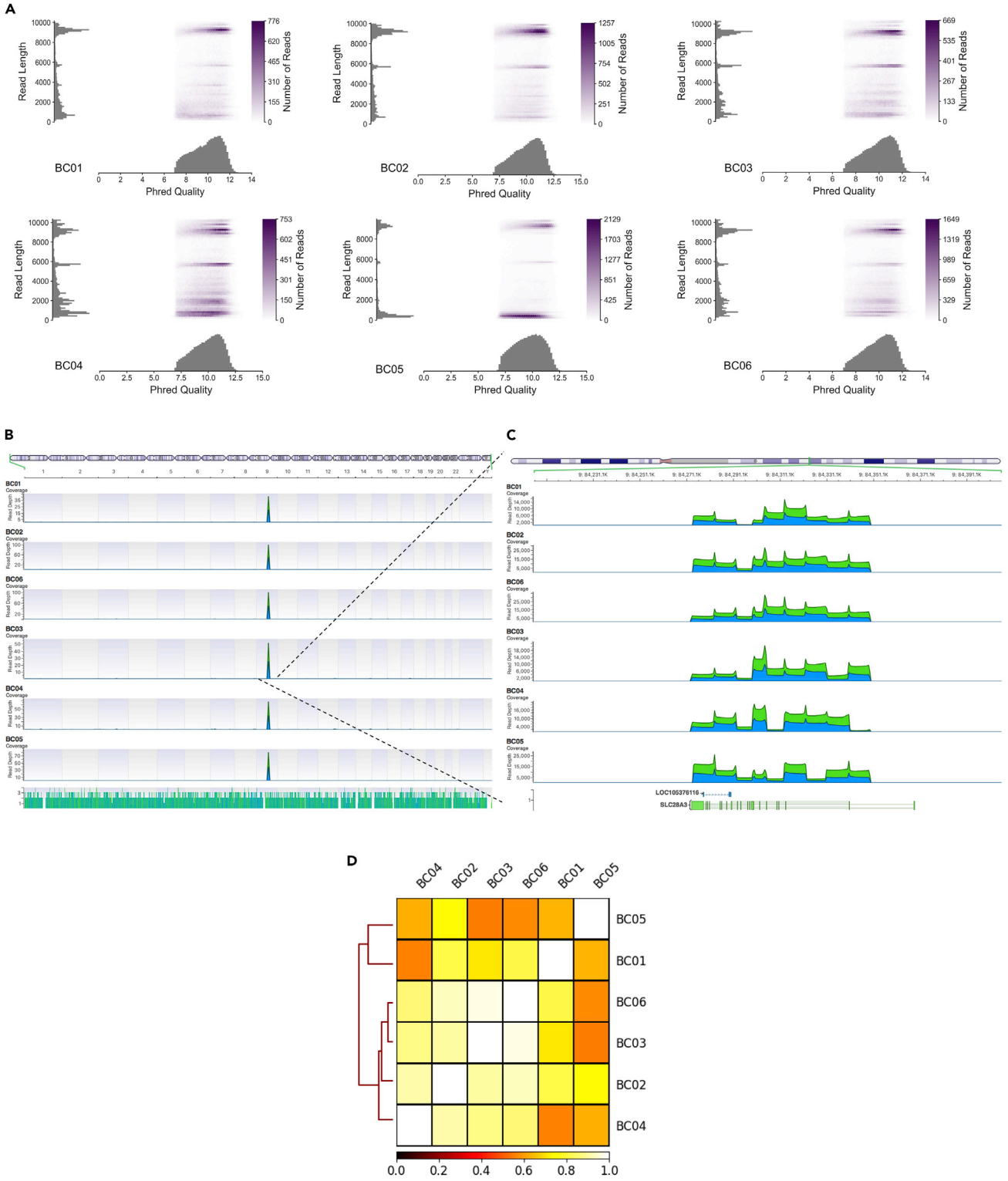

Figure 1. Nanopore Long Sequence Reads Encompassing *SLC28A3* Gene Locus

(A) Pauvre plot showing reads mean Phred quality score, reads length, and number of reads.

(B) Long-range PCR-based target enrichment for *SLC28A3* amplicons aligned to reference human genome (GRCh38) showing depth of coverage peaks at chr9: 84,274,029–84,349,802.

Figure 1. *Continued*

(C) Zoom-in view at locus chr9: 84,274,029–84,349,802 encompassing *SLC28A3*.

(D) Heatmap showing the correlation of the depth of coverage at *SLC28A3* locus between demultiplexed samples, BC01–BC06. The color code denotes value of Pearson correlation coefficient.

information for previously identified SNPs in a particular population; however, it is unable to identify novel variant that might be harbored by a study cohort.

Recently, Oxford Nanopore Technologies has introduced a single molecule-based portable sequencer, MinION. MinION is capable of generating ultra-long sequence reads (up to 200 kb) that improves alignment and assembly. Nanopore sequencing utilizes synthetic nanopore proteins that are embedded into an electrically resistant polymer membrane. Ionic current is generated by applying voltage across the membrane at the beginning of the experiment, and base calling is generated by recording the disruption in ionic current caused by each nucleotide passing through nanopore protein (Jain et al., 2016). MinION-derived long sequence reads have been successfully utilized to genotype single nucleotide variants (SNVs) and identify insertions, deletions, and translocations in different types of diseases (Lang et al., 2018; Patel et al., 2018; Fuselli et al., 2018). The long sequencing reads generated by nanopore technology provide cost-effective, high depth of coverage and phasing of identified variants. Moreover, real-time data analysis provides the privilege of controlling the utilization of the MinION flow cell, as the sequencing could be stopped once sufficient coverage is reached.

Another unique advantage of Nanopore long reads is the feasibility of variants phasing. Phasing by definition is the assignment of variant alleles to paternal or maternal chromosomes and thus adds more useful information from each Nanopore sequencing experiment. Phasing could help identify inheritance patterns, allele-specific expression, haplotype resolution, and disease risk haplotypes, and accordingly, it may compensate for the analysis of relatives in rare clinical research samples (Mantere et al., 2019). The success rate of short sequence reads-based phasing is ~20% because reliable phasing requires that heterozygous variants are covered by the same sequence read, which is a big limitation for short sequence reads (Goldmann et al., 2016). On contrary, Nanopore long reads facilitate phasing of genetic variants that are multiple kilobases apart directly from sequencing reads (Laver et al., 2016), as well as complex genomic regions such as the major histocompatibility complex (MHC) locus that encompasses 4 Mb (Jain et al., 2018).

Here, we use data from a recent large multi-center pediatric GWAS that revealed a candidate cardioprotective SNP (rs7853758, G>A, L461L) in *SLC28A3*, previously called human concentrative nucleoside transporter-3 (hCNT3), as significantly associated with lower risk to develop doxorubicin-induced cardiotoxicity (DIC) (Visscher et al., 2012). This GWAS hit, rs7853758, is a synonymous SNP and thus most likely is not the causal SNP. In this work we sought to introduce a Nanopore-based precise and cost-effective pipeline for multiplexed targeted resequencing that provides high-level (~500x) depth of coverage and helps identify potential causal SNP/haplotype.

RESULTS AND DISCUSSION

Nanopore Sequencing of *SLC28A3* and Long Sequence Reads Alignment

First, we PCR amplified and validated nine amplicons compassing *SLC28A3* gene (Figures S1A and S1B); we then sequenced the multiplexed amplicons from six patients using MinION Nanopore sequencer. Cumulative number of generated bases was 0.51, 1.1, 0.61, 0.87, 0.9, and 1.3 GB, and cumulative number of generated sequencing reads after demultiplexing was 103328, 182305, 117217, 195579, 226355, and 244678 reads, for DNA from patients BC01, BC02, BC03, BC04, BC05, and BC06, respectively (Figures S2A and S2B). Median read quality was 10, 10.2, 10.1, 10, 9.7, and 10.1 for BC01, BC02, BC03, BC04, BC05, and BC06, respectively (Figure 1A).

We next aligned sequence reads to reference human genome (GRCh38.p92) to check for non-specific PCR products. Aligning reads to reference genome resulted in a single peak encompassing *SLC28A3* gene locus in our six samples (Figures 1B and 1C). The median percent identity of aligned reads was 89%, 88.7%, 88.9%, 88.6%, 88.7%, and 88.8% for BC01, BC02, BC03, BC04, BC05, and BC06, respectively (Figure S3). The depth of coverage at *SLC28A3* locus for all samples was well correlated, in that average Pearson correlation co-efficient of one sample in relation to the other five samples was 0.7, 0.9, 0.86, 0.86, 0.7, and 0.87 for BC01,

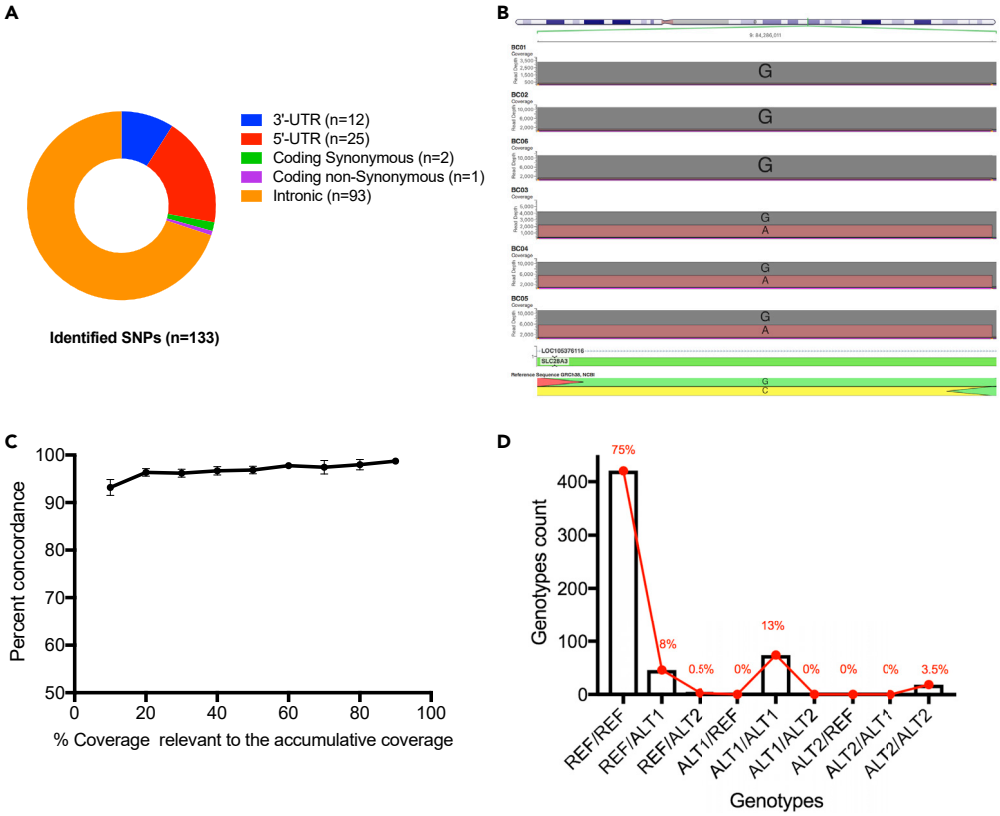

Figure 2. Variants Calling after *SLC28A3* Nanopore Sequencing

(A) Consequence and location of identified SNPs (n = 133).

(B) Aligned sequence reads at the location of the original GWAS hit (rs7853758, G>A, L461L) confirm that BC01, BC02, and BC06 harbor homozygous reference genotype (GG), whereas BC03, BC04, and BC05 harbor heterozygotes variant genotype (GA).

(C) Effect of depth of coverage on variant calling after Nanopore sequencing of study samples (n = 6). Sequence reads were down-sampled down to 10% of the cumulative read counts.

(D) Genotypes (n = 563) concordance between nanopore sequencing and SNP-chip technologies. The genotypes are homozygous reference (REF), heterozygous (ALT1), and homozygous non-reference (ALT2). Genotype pairs such as REF/REF represent genotype calls by nanopore and by the Omni chip, respectively. REF/REF, ALT1/ALT1, and ALT2/ALT2 indicate concordant genotypes. Line graph represents genotype percentage of total.

BC02, BC03, BC04, BC05, and BC06, respectively (Figure 1D). Taken together, homogeneous depth of coverage and read quality of all multiplexed samples along with the availability of a 96-barcoding kit maximizes the utility of this pipeline.

Variant Identification from Aligned Nanopore Long Sequence Reads

We next sought to identify SNPs in the study patients using Nanopolish (Loman et al., 2015) variant caller. In total 133 SNPs were identified, all of which have at least one variant allele in at least one patient (Figure 2A). The vast majority of identified SNPs are intronic (n = 93), 25 SNPs are located in 5′-UTR, 12 SNPs are located in 3′-UTR, in addition to three coding SNPs including two synonymous and one non-synonymous SNP (Figure 2A and Table S6). Of 133 identified SNPs, 28 are novel SNPs that have not been previously reported (Table S6). For all patients, Nanopore genotypes of the original GWAS hit, rs7853758, were in concordance with the GWAS-chip genotypes (Figure 2B). Novel SNPs included 14 intronic SNPs, 12 SNPs located in 5′-UTR, one SNP located in 3′-UTR, in addition to one non-synonymous SNP located at chr9:84285427 results in amino acid alteration Ala522Val (Table S6). The identified novel SNPs are co-inherited in both cardiotoxicity and cardioprotective patients and thus unlikely to be involved in doxorubicin-induced cardiotoxicity. However, identification of SNPs that are not captured by the GWAS SNP-chip is a major strength of the proposed pipeline, as these SNPs might have been missed if imputation only was implemented for fine-mapping.

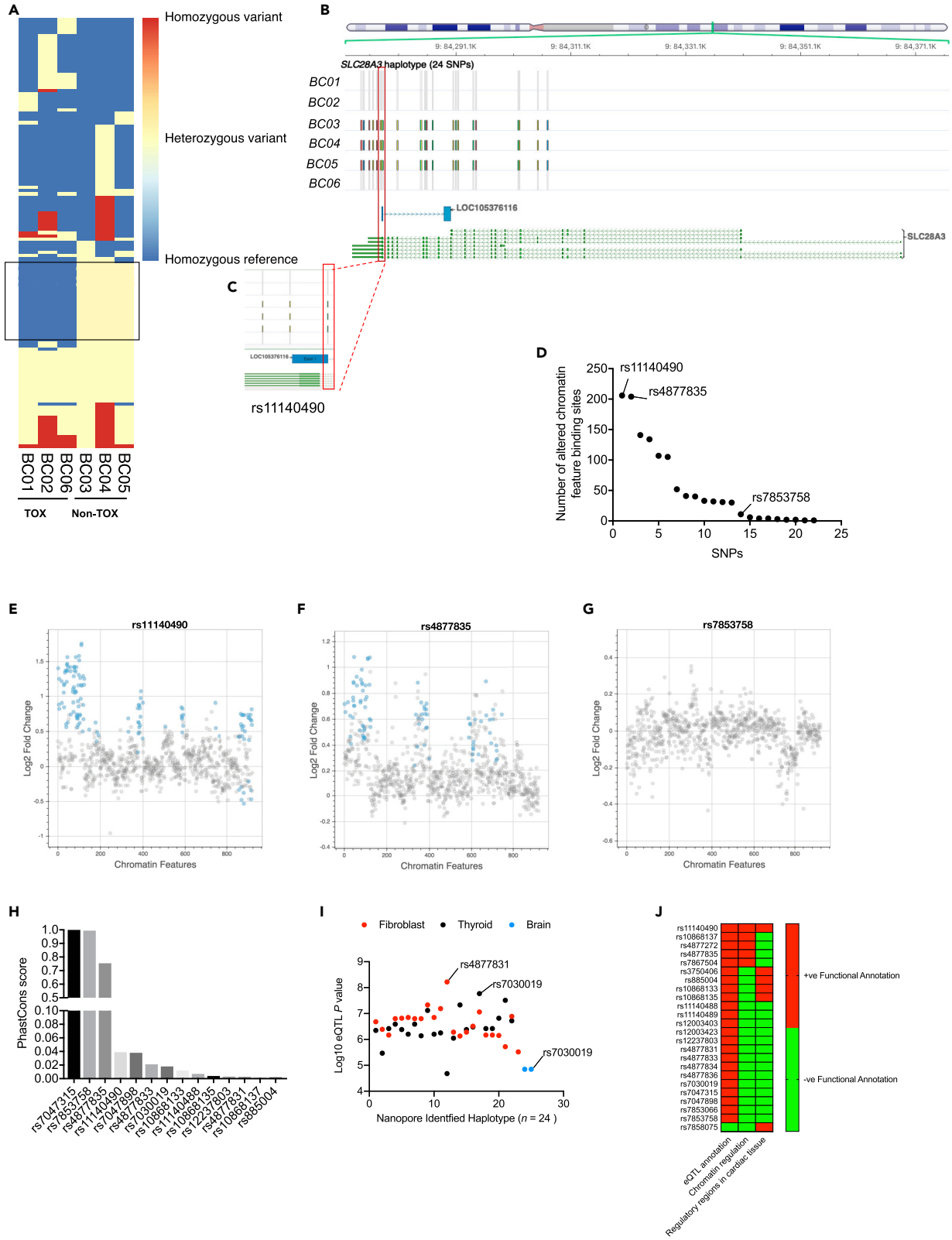
A
Homozygous variant
Heterozygous variant
Homozygous reference
BC01
BC02
BC06
BC03
BC04
BC05
TOX
Non-TOX
B
9: 84,291.1K
9: 84,311.1K
9: 84,331.1K
9: 84,351.1K
9: 84,371.1K
SLC28A3 haplotype (24 SNPs)
BC01
BC02
BC03
BC04
BC05
BC06
LOC105376116
SLC28A3
C
rs11140490
D
Number of altered chromatin feature binding sites
SNPs
rs11140490
rs4877835
rs7853758
E
rs11140490
Log2 Fold Change
Chromatin Features
F
rs4877835
Log2 Fold Change
Chromatin Features
G
rs7853758
Log2 Fold Change
Chromatin Features
H
PhastCons score
rs7047315
rs7853758
rs4877835
rs11140490
rs7047898
rs4877833
rs7030019
rs10868133
rs11140488
rs10868135
rs12237803
rs4877831
rs10868137
rs885004
I
Fibroblast
Thyroid
Brain
Log10 eQTL P value
rs4877831
rs7030019
rs7030019
Nanopore Identfied Haplotype (n = 24)
J
rs11140490
rs10868137
rs4877272
rs4877835
rs7867504
rs3750406
rs885004
rs10868133
rs10868135
rs11140488
rs11140489
rs12003403
rs12003423
rs12237803
rs4877831
rs4877833
rs4877834
rs4877836
rs7030019
rs7047315
rs7047898
rs7853066
rs7853758
rs7858075
+ve Functional Annotation
-ve Functional Annotation
eQTL annotation
Chromatin regulation
Regulatory regions in cardiac tissue

Figure 3. Identification of Potential Causal SNP after Nanopore Sequencing

(A) Heatmap showing identified SNP (n = 133) genotypes in all study patients (n = 6) after *SLC28A3* sequencing. A total of 133 SNPs have been identified, all of which have at least one variant allele in at least one of the study samples. SNPs (n = 24) marked on the heatmap by black rectangle are those that are coinherited in Non-TOX (no toxicity) samples but not in TOX (toxicity).

(B) The distribution of potential *SLC28A3* haplotype (24 SNPs) across *SLC28A3* and the overlapping long noncoding RNA, *AL356134.1*.

(C) Zoom-in view of SNP rs11140490 located in the splice site of the first exon of *AL356134.1*.

(D) Regulatory effect of candidate SNPs on chromatin feature binding sites.

(E–G) SNPs functional annotation using chromatin regulatory analysis for SNP rs11140490 (E), rs4877835 (F), and rs7853758 (G). Log2 fold change measures the fold change in the probability of observing a binding site for relevant chromatin feature between reference and alternative allele for a particular SNP (Zhou and Troyanskaya, 2015). Significant (E-value $\leq$0.02) predicted effect of a SNP on a particular chromatin feature binding site is denoted by blue dots.

(H) Conservation analysis of *SLC28A3* candidate SNPs using PhastCons database and SnpSift (Cingolani et al., 2012).

(I) eQTL annotation for candidate SNPs using Genotype-Tissue Expression (GTEx) project database.

(J) Overall prioritization of candidate causal SNPs based on functional annotation analyses including eQTL annotation, chromatin regulatory analyses, and overlapping with regulatory regions in cardiac tissues.

Effect of Depth of Coverage on Genotype Concordance Rate

To investigate how low coverage depth might affect variant calling from Nanopore reads, each bam file containing all sequence reads from a particular patient was down-sampled to include only 90%, 80%, 70%, 60%, 50%, 40%, 30%, 20%, and 10% of the accumulative reads. Then variants called from down-sampled bam files were compared with variants called from the main bam file that contains all accumulative reads. Lower depth of coverage did not show dramatic effect on Nanopore-based variant calling. The mean genotypes concordance rate across all six samples was 98.73%, 97.98%, 97.44%, 97.77%, 96.86%, 96.70%, 96.18%, 96.35%, and 93.19% with decreasing coverage depth from 100% down to 10% (Figure 2C). This finding shows that ~500x depth of coverage is sufficient for reliable variant calling from Nanopore sequence reads. Moreover, the cumulative yield of a single Nanopore flow cell ranges between 7 and 10 Gb, and thus, when coupled with the available barcoding kits, this pipeline could be used to examine several candidate loci in at least 96 multiplexed samples.

Genotype Concordance between Nanopore SNPs and InfiniumOmniExpress-24v1-2

We had access to chip-based 94 genotyped loci distributed across *SLC28A3* gene in the six patients we sequenced (n = 563, one genotype was missed in one sample), allowing us to check for concordance rate at these overlapping sites. Using SnpSift (Cingolani et al., 2012), we examined genotype concordance between the nanopore sequencing and InfiniumOmniExpress-24v1-2 genotyping chip. We found that 514 of the 563 overlapping genotypes were concordant (91.3%), i.e., both technologies called the same genotype (homozygous reference, heterozygous, or homozygous non-reference) at the same loci for a particular patient (Figure 2D and Table S7).

Functional Annotation Analysis Identifies Potential Causal SNP/Haplotype

We next examined which SNPs are linked in cardioprotected patients. Of the 133 identified SNPs, 24 SNPs including the GWAS hit are co-inherited in cardioprotected patients (Figure 3A and Table S6). These 23 SNPs are distributed as follows: eight SNPs are located in 3′ UTR, 14 SNPs are intronic, and 1 coding synonymous SNP (Figure 3B). Interestingly, seven SNPs are located within a long non-coding RNA, *AL356134.1*, that overlaps with *SLC28A3*. Moreover, SNP rs11140490 is located at the splice site of the first exon of *AL356134.1* (Figure 3C).

In order to narrow down the list of potential variants implicated in the cardioprotective phenotype after doxorubicin treatment, we investigated the regulatory properties of all non-coding candidate SNPs. Using ENCODE and Roadmap Epigenomics (Kundaje et al., 2015) data and DeepSEA (Zhou and Troyanskaya, 2015) algorithm, we examined the functional effect of each SNP on altering chromatin features (transcription factors, DNase hypersensitive site, and histone marks) binding sites. Among all SNPs, rs11140490 and rs4877835 have the most substantial regulatory effects as both SNPs have been predicted to be involved in altering the binding site of 206 and 204 chromatin features, respectively (Figures 3D and S4, Tables S8 and S9). In that, SNP rs11140490 is predicted to alter the binding sites of 43 features with log2 fold change of $\geq$ 1 (Figure 3E), whereas rs4877835 is predicted to alter the binding sites of only four features with log2 fold change of $\geq$ 1 (Figure 3F). Importantly, the primary GWAS significant association does not show any chromatin regulatory effect (Figure 3G).

Since doxorubicin-induced cardiotoxicity affects mainly heart cells, we then performed an additional regulatory analysis exclusively focusing on human cardiac tissue, and for that we used ensemble regulatory

build that includes transcription factors, histone mark, and DNase hypersensitive regions. Six SNPs, rs11140490, rs4877835, rs4877831, rs7047898, rs885004, and rs10868137, are found to be located in at least one regulatory region in human cardiac tissue (Table S10 and Figure S5).

Then using phastCons database and SnpSift (Cingolani et al., 2012), we checked which of candidate SNPs are located in a highly conserved locus. We found that SNP rs4877835 is located in a highly conserved locus as compared with rs11140490, and rs10868137 with a conservation score of 0.75, 0.04, and 0.001, respectively (Figure 3H).

Finally, to investigate further regulatory consequences of these candidate SNPs, we used the Genotype-Tissue Expression (GTEx) project database (https://www.gtexportal.org/home/) and investigated which of the identified candidate SNPs have been shown to be an expression quantitative trait loci (eQTL). Almost all of the candidate SNPs have been previously identified as eQTL in cultured fibroblasts, thyroid, and brain tissues. In that, SNP rs4877831 is the most significant eQTL in cultured fibroblasts and SNP rs7030019 is the most significant eQTL in both thyroid and brain tissues (Figure 3I and Table S11).

These findings when taken together suggest that rs11140490 is the SNP with the highest likelihood to be causal. However, other candidate SNPs with positive functional annotations might also have a protective role against DIC (Figure 3J). SNP rs11140490 alone or in interaction with other identified candidate SNPs revealed from this analysis (Figure 3J) could affect the transcription and/or expression of *AL356134.1*, which regulates the expression of doxorubicin-related genes including *SLC28A3* and eventually regulates patients' susceptibility to doxorubicin-induced cardiotoxicity.

Fine-Mapping at *SLC28A3* Locus Using Genotype Imputation

We next sought to compare Nanopore-based fine mapping and imputation-based fine mapping at the *SLC28A3* locus. The original GWAS that identified SNP rs7853758 used a genotyping chip that covers ~2,000 SNPs across 220 ADME (absorption, distribution, metabolism, and excretion)-related genes, which included 23 SNPs distributed across SLC28A3 (Visscher et al., 2012). Genotype imputation of additional SNPs not present on the GWAS genotyping platform was done using SHAPEIT (Delaneau et al., 2011) for phasing followed by IMPUTE2 (Howie et al., 2009) with 1K genomes reference panel. To validate the imputation analysis, known GWAS genotypes were masked one variant at a time and imputed using the remaining study and reference data. Internal cross-validation showed that the mean concordance between imputed genotypes (including the original GWAS hit, rs7853758) and the original genotypes was 98.5% (Table S12).

In total, 817 additional SNPs were imputed with an accuracy ranging from 0%–100%. In that, 73 SNPs were imputed with at least 90% accuracy and 52 SNPs were imputed with at least 99% accuracy (Figure 4A). Schurz et al. among others showed that imputation accuracy significantly decreases with lower minor allele frequency (MAF) SNP (Schurz et al., 2019). Similarly, we have noticed that imputation accuracy is inversely correlated with SNPs MAF, emphasizing the value of the Nanopore-based pipeline in identifying rare variants that could have been otherwise missed (Figure 4B). We then focused on the Nanopore-identified cardioprotective haplotype (24 SNPs) that is co-inherited in cardioprotected patients. Only 19 SNPs within this haplotype were imputed in the study cohort (Figure 4C), whereas five SNPs that have been identified with the Nanopore pipeline were not imputed. Although the European population represented by this study cohort has substantial long LD haplotype stretches, imputation was not able to identify all SNPs identified by Nanopore sequencing at the investigated candidate locus. Thus, we believe that Nanopore sequencing pipeline provides a comprehensive fine-mapping approach specially when studying populations with higher recombination rates and shorter haplotype stretches such as the African population. Similarly, Nanopore pipeline is very useful when studying cohorts with no available reference panel. When analyzing such cohorts and in case of any limitation that prohibits sequencing all the cohort samples, a subset of samples might be sequenced at interesting loci using the Nanopore pipeline, and the generated data could serve as a reference panel for this particular cohort and is subsequently used for imputation-based fine-mapping for the rest of the cohort samples.

Haplotype Structure of *SLC28A3* Locus in Control Individuals ($n = 99$)

In order to confirm the linkage disequilibrium pattern of the Nanopore-identified cardioprotective haplotype (24 SNPs), we investigated the structure of this haplotype in 99 whole-genome sequenced control individuals from the CEU (Utah Residents [CEPH] with Northern and Western European Ancestry) population. The 24 SNPs constituting this cardioprotective haplotype are in high LD with an average D′ and R^2 of 0.99 and 0.84, respectively

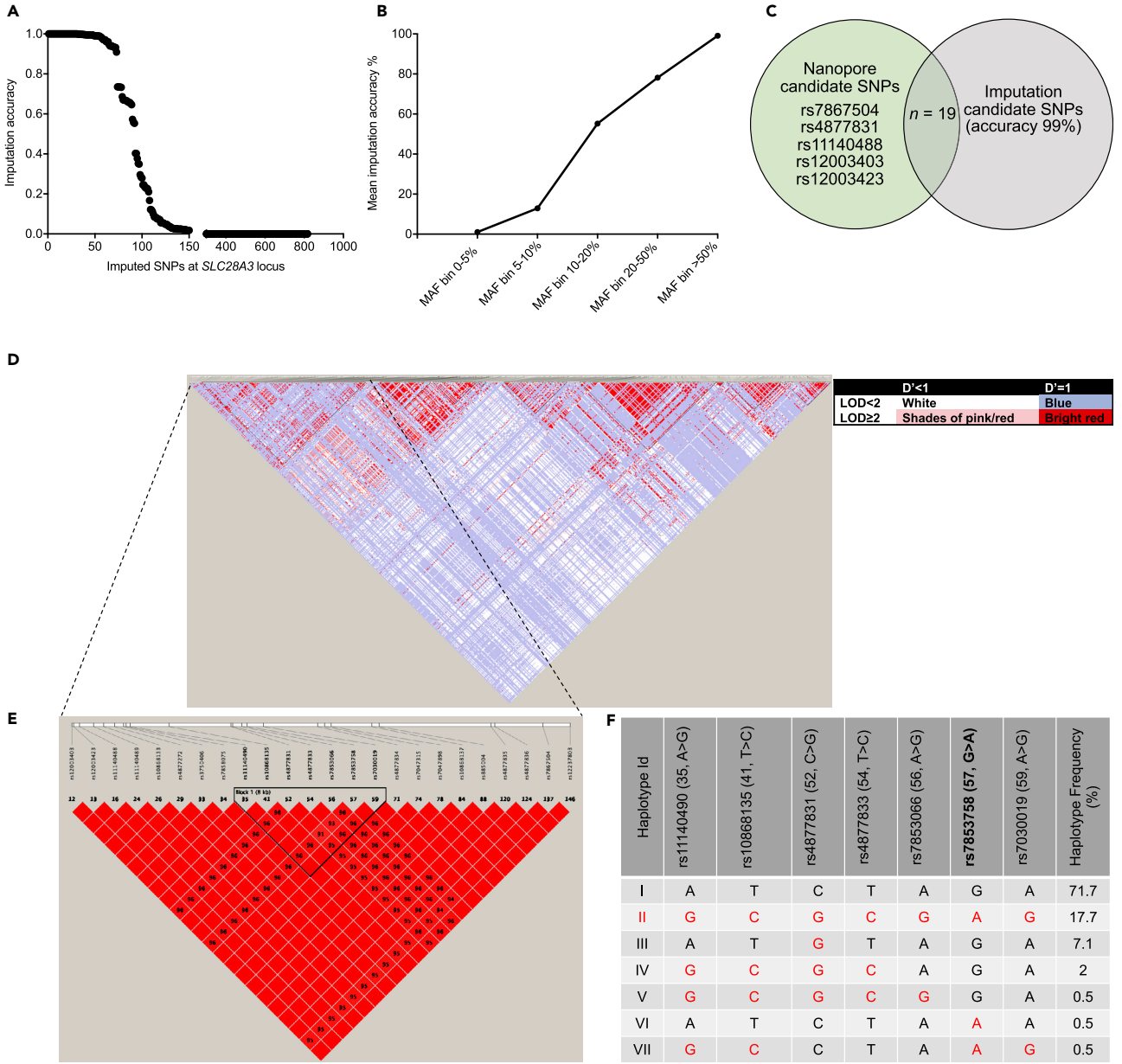

Haplotype Id	rs11140490 (35, A>G)	rs10868135 (41, T>C)	rs4877831 (52, C>G)	rs4877833 (54, T>C)	rs7853066 (56, A>G)	**rs7853758 (57, G>A)**	rs7030019 (59, A>G)	Haplotype Frequency (%)
I	A	T	C	T	A	G	A	71.7
II	G	C	G	C	G	A	G	17.7
III	A	T	G	T	A	G	A	7.1
IV	G	C	G	C	A	G	A	2
V	G	C	G	C	G	G	A	0.5
VI	A	T	C	T	A	A	A	0.5
VII	G	C	C	T	A	A	G	0.5

Figure 4. Genetic Analysis at *SLC28A3* Candidate Locus in Control Individuals

(A and B) (A) Genotype imputation of additional SNPs not present on the original GWAS genotyping platform. Genotype imputation was done using SHAPEIT for phasing followed by IMPUTE2 (Howie et al., 2009) with 1K genomes reference panel. (B) Imputation accuracy is inversely correlated with MAF. (C) Comparison between Nanopore pipeline-identified candidate SNPs (n = 24) and imputation-based identified SNPs (n = 19) at *SLC28A3* locus. (D–F) Haplotype structure of *SLC28A3* locus in control individuals (n = 99). (D) Pairwise linkage disequilibrium (D′) for all SNPs spread over ~100 kb encompassing *SLC28A3* locus. The linkage disequilibrium (D′) is indicated in the small boxes colored red or blue (a color legend is provided). LOD, log of the likelihood odds ratio. (E) LD haplotype structure for Nanopore-identified haplotype that is spread over 32 kb and comprises 24 SNPs that are co-inherited only in cardioprotected patients. The reference SNP numbers (rs) are indicated on top. Haplotype Block 1 (outlined by black triangle) is spread over 8 kb and is composed of seven SNPs that are located within a long non-coding RNA (LNCRNA), *AL356134.1*, that overlaps with *SLC28A3*. (F) The cardioprotective haplotype allelic frequencies in control individuals. Each SNP is labeled as follow: rs id (SNP number on the LD block in [B], reference allele > variant allele). SNP rs7853758 (in bold) is the primary GWAS hit. For each SNP, variant alleles are in red. Haplotype II that includes the variant alleles for all the seven SNPs have an allelic frequency of 17.7% in the CEU population. VCF file containing genotype calls for 99 CEU individuals was downloaded from the 1,000 genomes database for the 9p21.3 locus (chr9:84274029–84349802). Using VCFtools, VCF was converted to PED and MAP files. Plink (Purcell et al., 2007) was used to calculate linkage disequilibrium between SNPs, and finally the haplotype LD map was generated using Haploview V4.2.

(Figures 4D and 4E, and Table S13). Seven SNPs of the main haplotype are located within a long non-coding RNA (LNCRNA), *AL356134.1*, that overlaps with *SLC28A3,* forming a sub-haplotype block (Figure 4E). The seven SNPs that constitute this sub-haplotype are rs11140490 (A>G), rs10868135 (T>C), rs4877831 (C>G), rs4877833 (T>C), rs7853066 (A>G), rs7853758 (G>A), and rs7030019 (A>G).

We next investigated the allelic frequency of the *AL356134.1* overlapping sub-haplotype. Seven structural Haplotype I-VII were identified (Figure 4F), in that Haplotype I comprises the reference alleles for all seven SNPs (ATCTAGA) and is inherited in 71.7% of the examined population, whereas haplotype II is built of the variants alleles for all seven SNPs (GCGCGAG) and is inherited in 17.7% of the examined population (Figure 4F). This finding is consistent with the linkage disequilibrium pattern identified by the Nanopore pipeline.

Nanopore Pipeline Is a Cost-Effective Pipeline for Candidate Loci Sequencing

A standard single MinION flow cell run (48 h) generates 4–8 Gb of useful sequencing data, and herein we were able to generate ~6 Gb from one flow cell. Although the newer generation of MinION flow cells are able to generate up to 30 Gb of sequencing data in a single run (https://nanoporetech.com/products/comparison), the cost estimates calculated here are based on an output of 5 Gb per flow cell. The generated 5 Gb are equivalent to 10 Mb with a depth of coverage of 500x that is suitable for downstream variant calling. The availability of Nanopore barcoding kits enables the multiplexing of up to 96 samples. One MinION flow cell generates 10 Mb (500x coverage) and thus is enough to sequence ~104 kb (500x coverage) in 96 samples that costs as low as $8/sample. This cost includes the cost of the MinION sequencer, MinION flow cell, library preparation, and samples barcoding. Nanopore sequencing for candidate loci is thus significantly more cost-effective as compared to other sequencing approaches including the commonly used Illumina targeted sequencing that costs ~$50/sample. These cost estimates do not include the cost of the Miseq Illumina sequencer, which is about $125,000. On contrary, the Nanopore MinION sequencer is included in a basic starter kit that also includes two flow cells and a sequencing kit all of which costs $1,000. A detailed cost estimates for Nanopore sequencing and Illumina targeted sequencing are mentioned in Table S14.

In summary, Nanopore long-read sequences coupled with long-range PCR comprises a useful aide for comprehensive post-GWAS fine-mapping and helps identification of causal SNP/haplotype. Using the herein introduced pipeline, 100 kb candidate loci sequencing with ample depth of coverage of 500x, that is compatible with reliable downstream variant calling would cost ~$10/sample. Real-time analysis of Nanopore sequencing run makes other permutations such as examining bigger candidate loci and smaller number of samples also possible at similar cost. Nanopore-based fine-mapping is able to prioritize candidate causal SNPs and is more comprehensive as compared with imputation-based fine mapping. The Nanopore-based approach eliminates the need for costly traditional post-GWAS resequencing strategies while still providing extensive information for examined genetic loci. Fine-mapping approaches, weather it is statistics based or functional annotation based when coupled to our pipeline that provides high-density genotyping information, will substantially help prioritization and identification of causal SNPs. The constant improvement in long reads aligning and variant calling algorithms will definitely expand the utility of this pipeline in the future.

Limitation of the Study

In this work we provide a proof of principle for the application of Nanopore sequencing in post-GWAS fine-mapping and pinpointing of potential causal SNPs. However, low sample size is a limitation of our study. Herein, six well-phenotyped, doxorubicin-exposed patients from the Canadian cohort were specifically re-recruited according to the original inclusion criteria. Re-recruiting more patients with similar strict criteria is very challenging and time consuming. Our proposed pipeline is worth testing in a larger cohort.

METHODS

All methods can be found in the accompanying Transparent Methods supplemental file.

DATA AND CODE AVAILABILITY

The data that support the findings of this study are available from the corresponding author upon reasonable request.

SUPPLEMENTAL INFORMATION

Supplemental Information can be found online at https://doi.org/10.1016/j.isci.2020.100971.

ACKNOWLEDGMENTS

This work was supported by NIH grant R01 CA220002, American Heart Association Transformational Project Award 18TPA34230105, a Dixon Foundation Translational Research Grants Innovation Award, and the Fondation Leducq (P.W.B.).

AUTHOR CONTRIBUTIONS

P.W.B. supervised the project. P.W.B. and T.M. conceived the project and wrote the paper. T.M. completed most of the experiment along with H.-H.K. T.M. completed the bioinformatics analysis.

DECLARATION OF INTERESTS

The authors have no conflicts of interest to declare.

Received: August 30, 2019
Revised: January 13, 2020
Accepted: March 5, 2020
Published: April 24, 2020

REFERENCES

Abecasis, G.R., Auton, A., Brooks, L.D., Depristo, M.A., Durbin, R.M., Handsaker, R.E., Kang, H.M., Marth, G.T., and Mcvean, G.A. (2012). An integrated map of genetic variation from 1,092 human genomes. Nature *491*, 56–65.

Altshuler, D.M., Altshuler, D.M., Gibbs, R.A., Peltonen, L., Altshuler, D.M., Gibbs, R.A., Peltonen, L., Dermitzakis, E., Schaffner, S.F., Yu, F., et al. (2010). Integrating common and rare genetic variation in diverse human populations. Nature *467*, 52–58.

Browning, S.R. (2008). Missing data imputation and haplotype phase inference for genome-wide association studies. Hum. Genet. *124*, 439–450.

Cingolani, P., Patel, V.M., Coon, M., Nguyen, T., Land, S.J., Ruden, D.M., and Lu, X. (2012). Using *Drosophila melanogaster* as a model for genotoxic chemical mutational studies with a new program, SnpSift. Front. Genet. *3*, 35.

Delaneau, O., Marchini, J., and Zagury, J.F. (2011). A linear complexity phasing method for thousands of genomes. Nat. Methods *9*, 179–181.

Fuselli, S., Baptista, R.P., Panziera, A., Magi, A., Guglielmi, S., Tonin, R., Benazzo, A., Bauzer, L.G., Mazzoni, C.J., and Bertorelle, G. (2018). A new hybrid approach for MHC genotyping: high-throughput NGS and long read MinION nanopore sequencing, with application to the non-model vertebrate Alpine chamois (*Rupicapra rupicapra*). Heredity (Edinb) *121*, 293–303.

Genomes Project, C., Abecasis, G.R., Altshuler, D., Auton, A., Brooks, L.D., Durbin, R.M., Gibbs, R.A., Hurles, M.E., and Mcvean, G.A. (2010). A map of human genome variation from population-scale sequencing. Nature *467*, 1061–1073.

Goldmann, J.M., Wong, W.S., Pinelli, M., Farrah, T., Bodian, D., Stittrich, A.B., Glusman, G., Vissers, L.E., Hoischen, A., Roach, J.C., et al. (2016). Parent-of-origin-specific signatures of de novo mutations. Nat. Genet. *48*, 935–939.

Howie, B.N., Donnelly, P., and Marchini, J. (2009). A flexible and accurate genotype imputation method for the next generation of genome-wide association studies. PLoS Genet. *5*, e1000529.

Jain, M., Koren, S., Miga, K.H., Quick, J., Rand, A.C., Sasani, T.A., Tyson, J.R., Beggs, A.D., Dilthey, A.T., Fiddes, I.T., et al. (2018). Nanopore sequencing and assembly of a human genome with ultra-long reads. Nat. Biotechnol. *36* (4), 338–345.

Jain, M., Olsen, H.E., Paten, B., and Akeson, M. (2016). The Oxford Nanopore MinION: delivery of nanopore sequencing to the genomics community. Genome Biol. *17*, 239.

Konig, I.R., Loley, C., Erdmann, J., and Ziegler, A. (2014). How to include chromosome X in your genome-wide association study. Genet. Epidemiol. *38*, 97–103.

Kundaje, A., Meuleman, W., Ernst, J., Bilenky, M., Yen, A., Heravi-Moussavi, A., Kheradpour, P., Zhang, Z., Wang, J., Ziller, M.J., et al. (2015). Integrative analysis of 111 reference human epigenomes. Nature *518*, 317–330.

Lang, K., Surendranath, V., Quenzel, P., Schofl, G., Schmidt, A.H., and Lange, V. (2018). Full-length HLA class I genotyping with the MinION nanopore sequencer. Methods Mol. Biol. *1802*, 155–162.

Laver, T.W., Caswell, R.C., Moore, K.A., Poschmann, J., Johnson, M.B., Owens, M.M., Ellard, S., Paszkiewicz, K.H., and Weedon, M.N. (2016). Pitfalls of haplotype phasing from amplicon-based long-read sequencing. Sci. Rep. *6*, 21746.

Loman, N.J., Quick, J., and Simpson, J.T. (2015). A complete bacterial genome assembled de novo using only nanopore sequencing data. Nat. Methods *12*, 733–735.

MacArthur, J., Bowler, E., Cerezo, M., Gil, L., Hall, P., Hastings, E., Junkins, H., McMahon, A., Milano, A., Morales, J., et al. (2017). The new NHGRI-EBI Catalog of published genome-wide association studies (GWAS Catalog). Nucleic Acids Res. *45*, D896–D901.

Magdy, T., Burmeister, B.T., and Burridge, P.W. (2016). Validating the pharmacogenomics of chemotherapy-induced cardiotoxicity: what is missing? Pharmacol. Ther. *168*, 113–125.

Magdy, T., and Burridge, P.W. (2018). The future role of pharmacogenomics in anticancer agent-induced cardiovascular toxicity. Pharmacogenomics *19*, 79–82.

Mantere, T., Kersten, S., and Hoischen, A. (2019). Long-read sequencing emerging in medical genetics. Front. Genet. *10*, 426.

Marchini, J., and Howie, B. (2010). Genotype imputation for genome-wide association studies. Nat. Rev. Genet. *11*, 499–511.

Patel, A., Belykh, E., Miller, E.J., George, L.L., Martirosyan, N.L., Byvaltsev, V.A., and Preul, M.C. (2018). MinION rapid sequencing: Review of potential applications in neurosurgery. Surg. Neurol. Int. *9*, 157.

Purcell, S., Neale, B., Todd-Brown, K., Thomas, L., Ferreira, M.A., Bender, D., Maller, J., Sklar, P., de Bakker, P.I., Daly, M.J., et al. (2007). PLINK: a tool set for whole-genome association and population-based linkage analyses. Am. J. Hum. Genet. *81*, 559–575.

Roshyara, N.R., Horn, K., Kirsten, H., Ahnert, P., and Scholz, M. (2016). Comparing performance of modern genotype imputation methods in different ethnicities. Sci. Rep. *6*, 34386.

Schurz, H., Muller, S.J., Van Helden, P.D., Tromp, G., Hoal, E.G., Kinnear, C.J., and Moller, M. (2019). Evaluating the accuracy of imputation methods in a five-way admixed population. Front. Genet. *10*, 34.

Visscher, H., Ross, C.J., Rassekh, S.R., Barhdadi, A., Dubé, M.P., Al-Saloos, H., Sandor, G.S., Caron, H.N., van Dalen, E.C., Kremer, L.C., et al. (2012). Pharmacogenomic prediction of anthracycline-induced cardiotoxicity in children. J. Clin. Oncol. *30*, 1422–1428.

Zhou, J., and Troyanskaya, O.G. (2015). Predicting effects of noncoding variants with deep learning-based sequence model. Nat. Methods *12*, 931–934.

iScience, Volume *23*

Supplemental Information

Precise and Cost-Effective Nanopore Sequencing for Post-GWAS Fine-Mapping and Causal Variant Identification

Tarek Magdy, Hui–Hsuan Kuo, and Paul W. Burridge

A

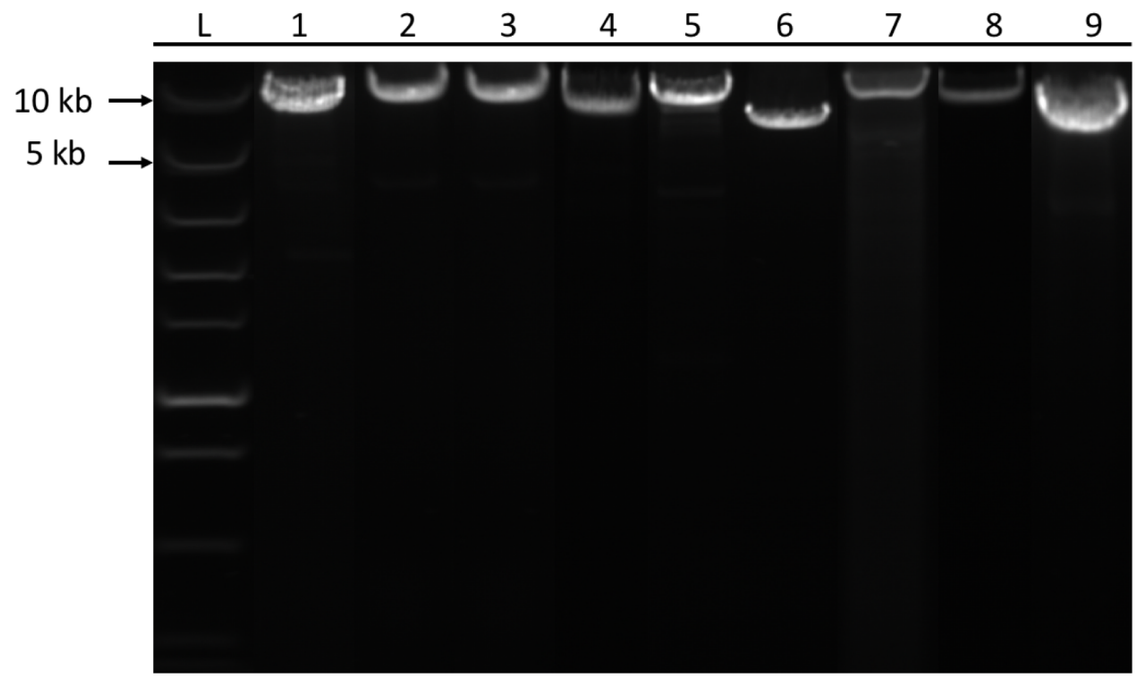
L
1
2
3
4
5
6
7
8
9
10 kb
5 kb

B

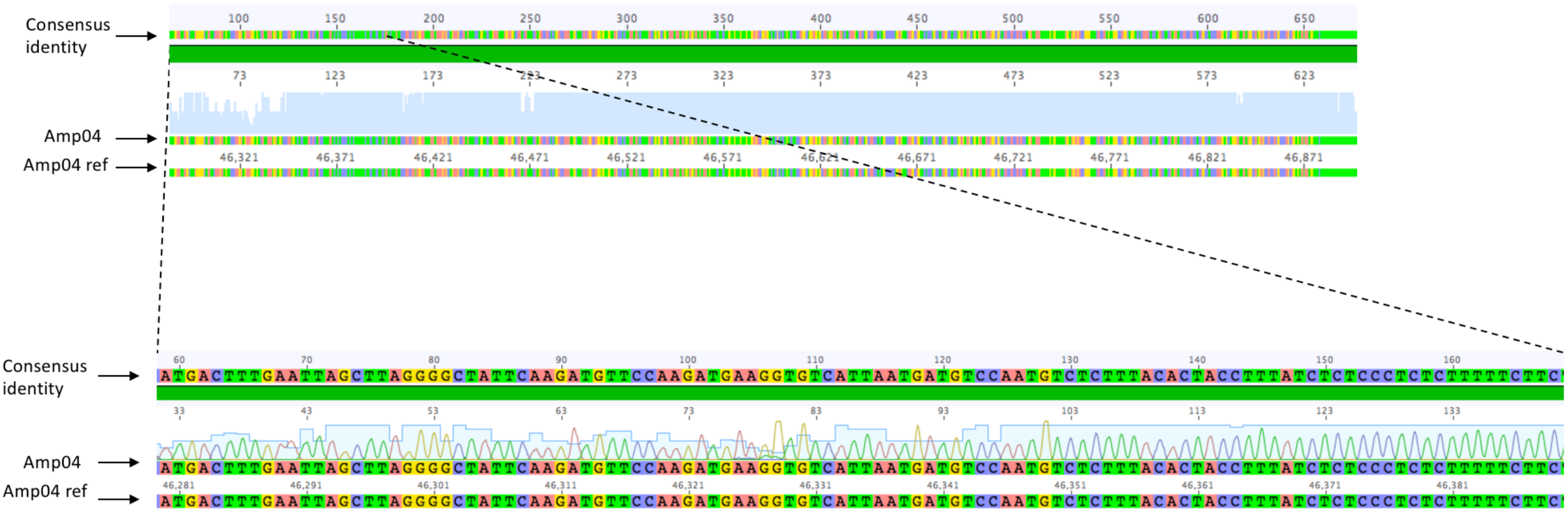
Consensus identity
Amp04
Amp04 ref
Consensus identity
Amp04
Amp04 ref

Figure S1

(a)

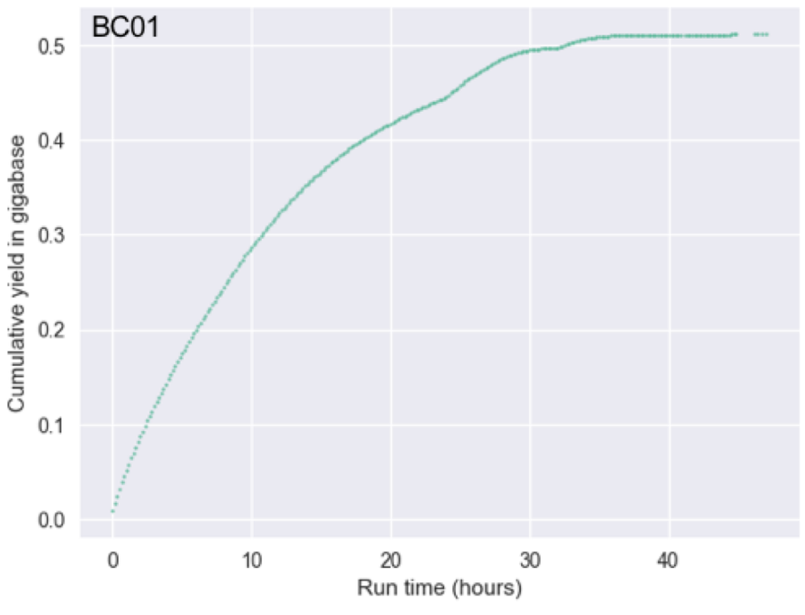
BC01
Cumulative yield in gigabase
Run time (hours)

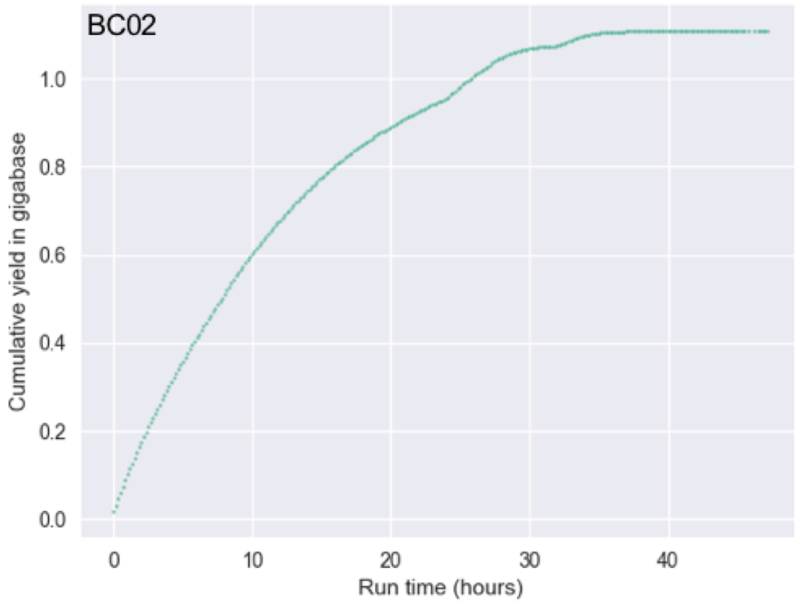
BC02
Cumulative yield in gigabase
Run time (hours)

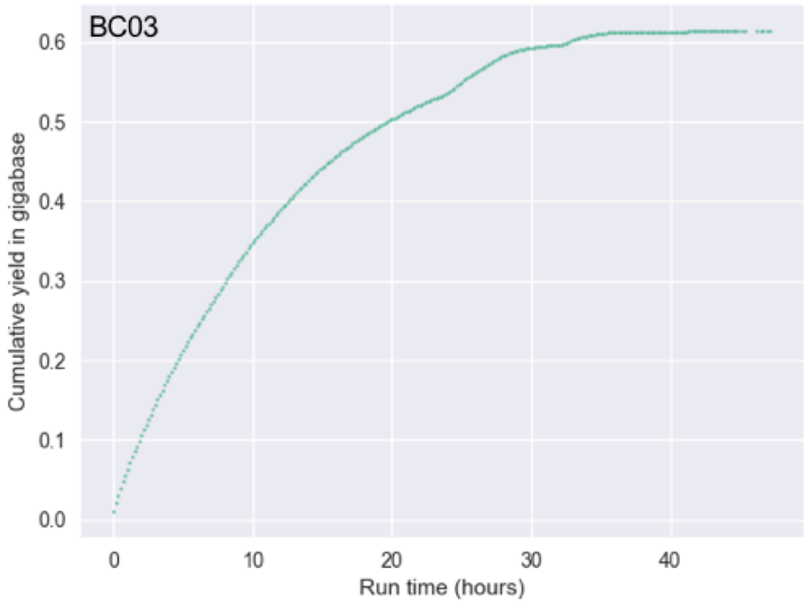
BC03
Cumulative yield in gigabase
Run time (hours)

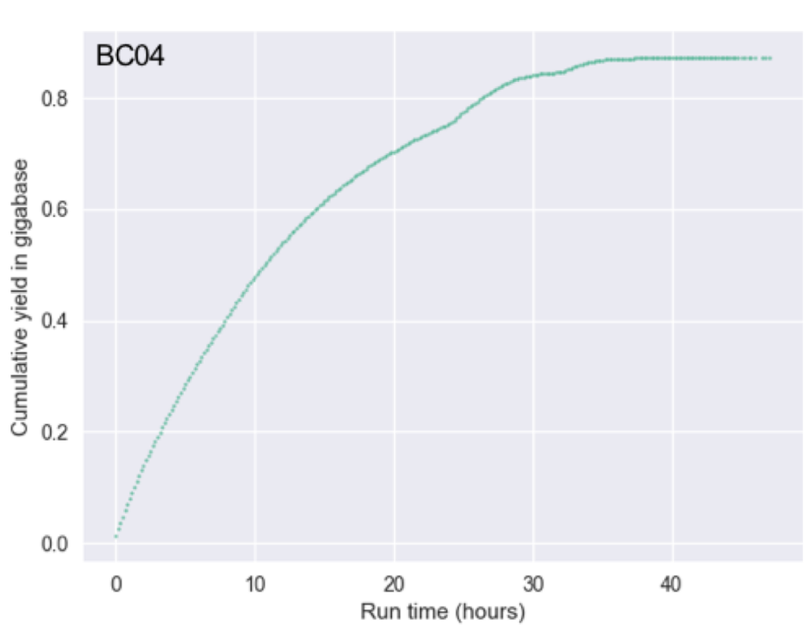
BC04
Cumulative yield in gigabase
Run time (hours)

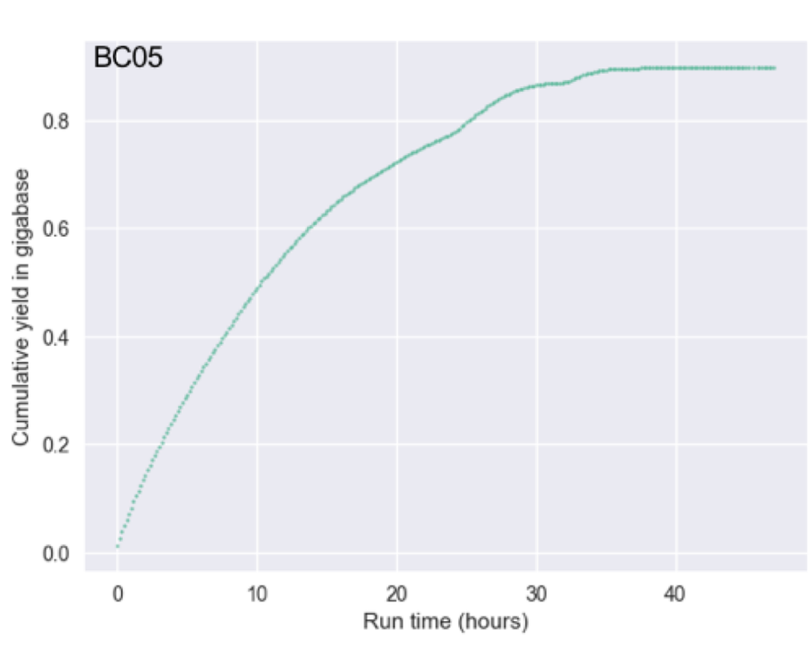
BC05
Cumulative yield in gigabase
Run time (hours)

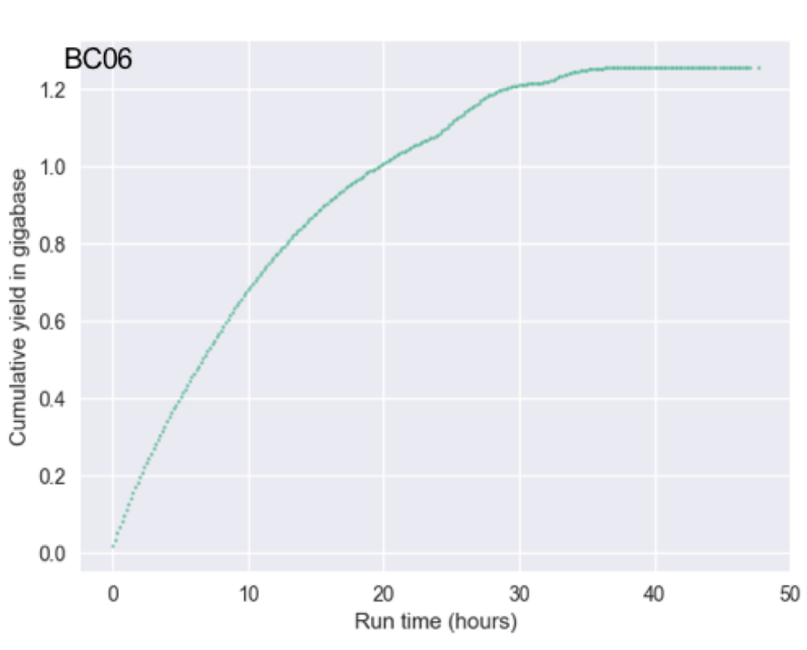
BC06
Cumulative yield in gigabase
Run time (hours)

(b)

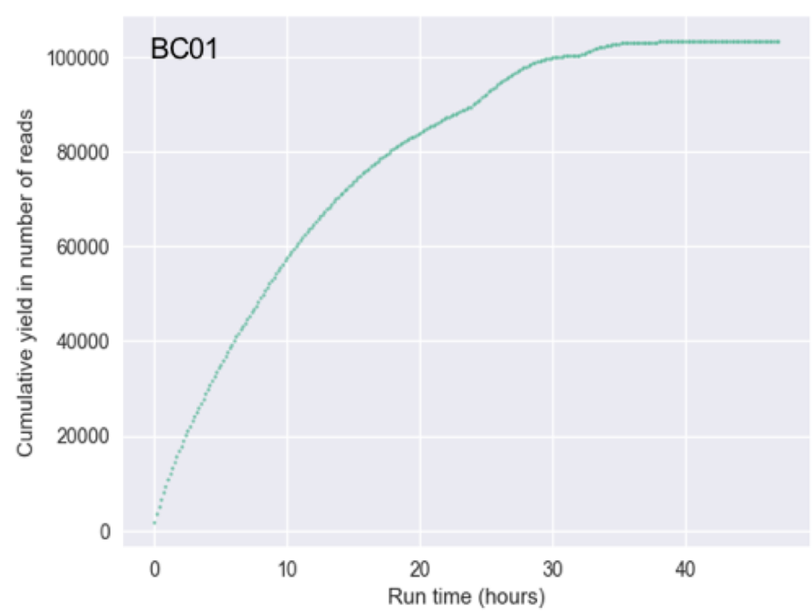
BC01
Cumulative yield in number of reads
Run time (hours)

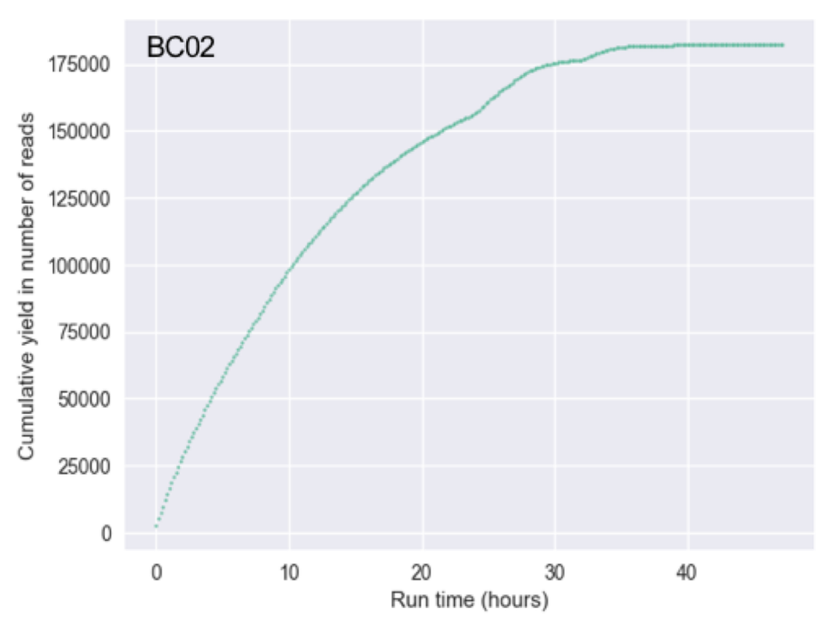
BC02
Cumulative yield in number of reads
Run time (hours)

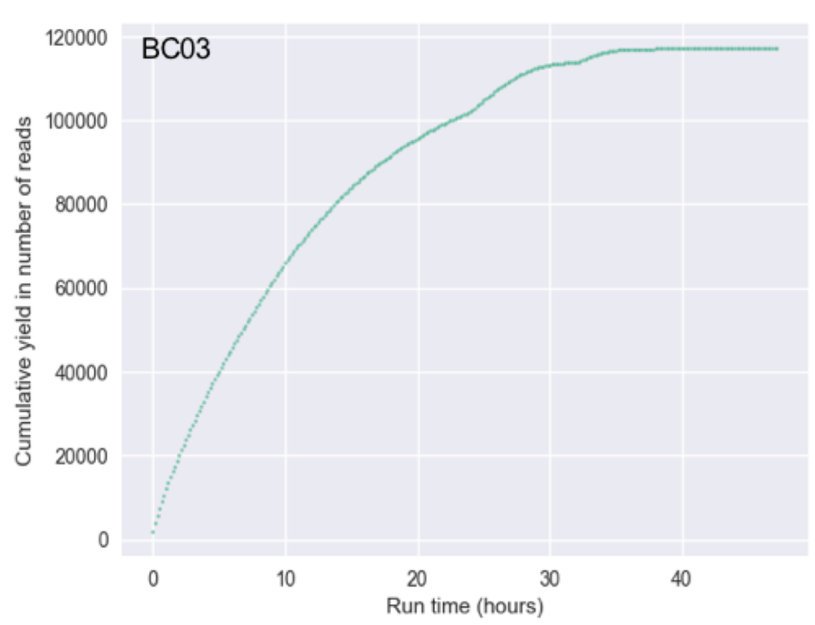
BC03
Cumulative yield in number of reads
Run time (hours)

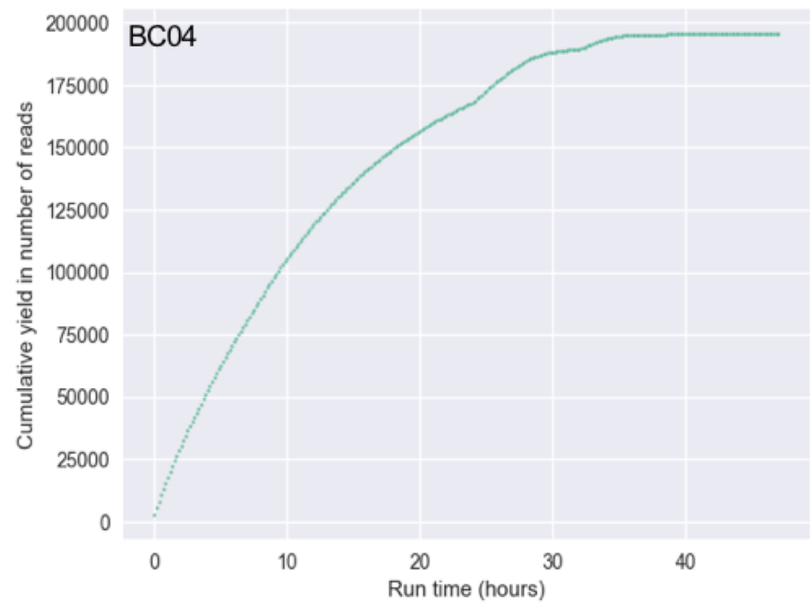
BC04
Cumulative yield in number of reads
Run time (hours)

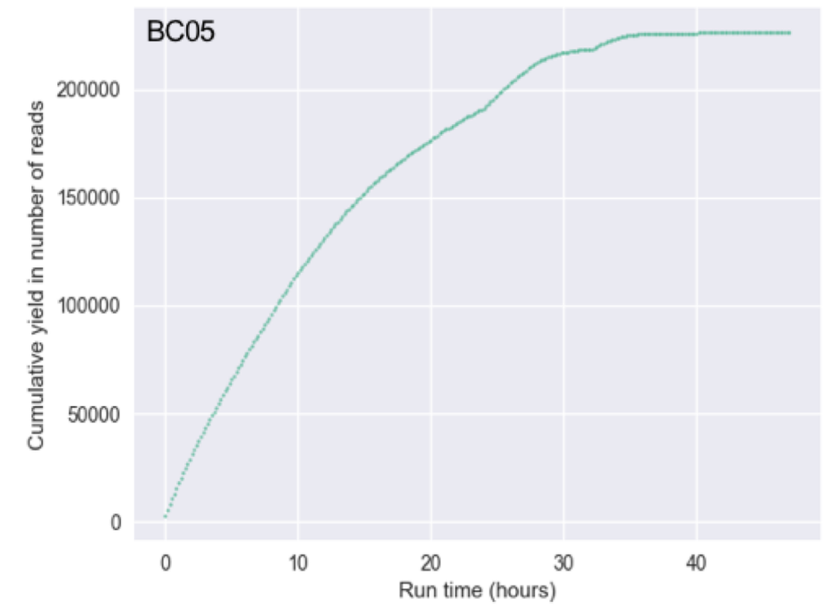
BC05
Cumulative yield in number of reads
Run time (hours)

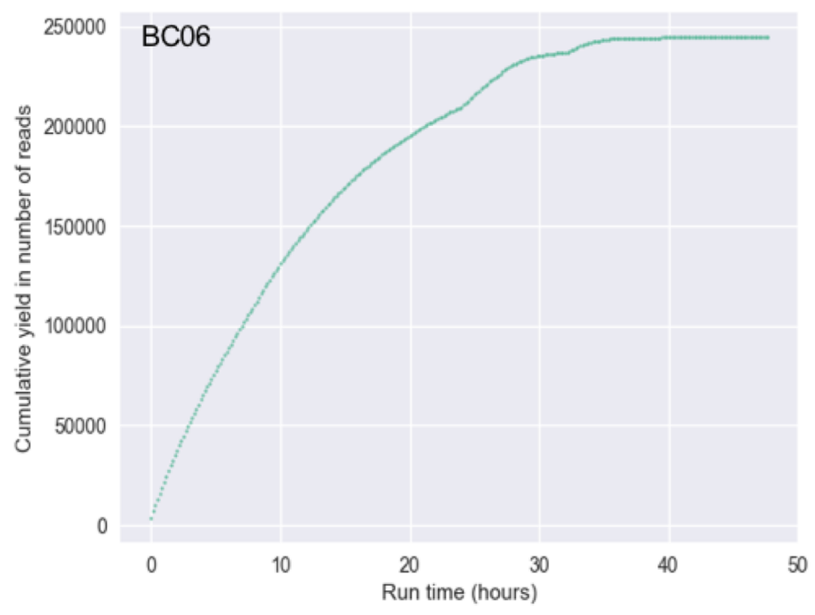
BC06
Cumulative yield in number of reads
Run time (hours)

Figure S2

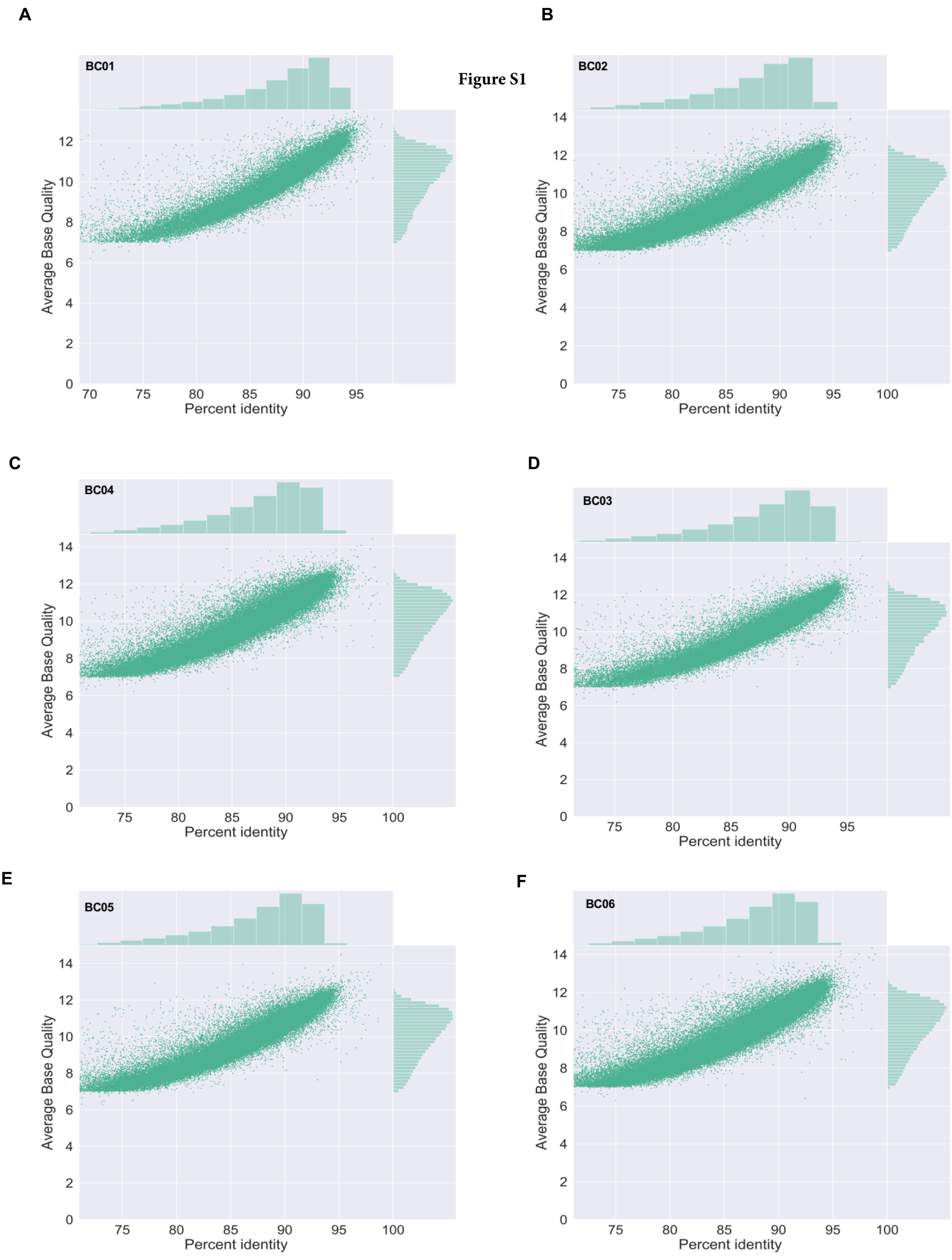

Figure S1

Figure S3

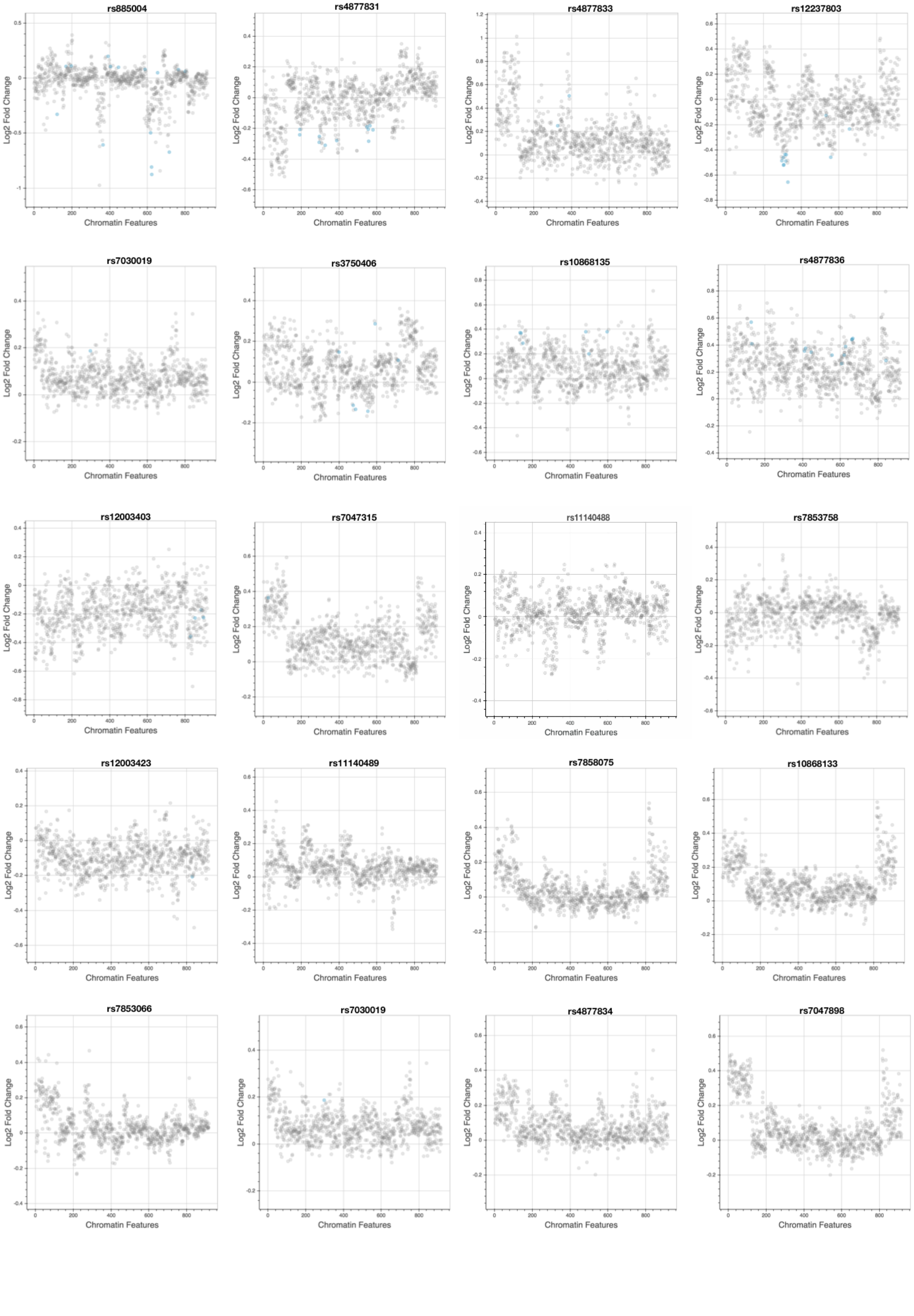
rs885004
rs4877831
rs4877833
rs12237803
rs7030019
rs3750406
rs10868135
rs4877836
rs12003403
rs7047315
rs11140488
rs7853758
rs12003423
rs11140489
rs7858075
rs10868133
rs7853066
rs7030019
rs4877834
rs7047898
Log2 Fold Change
Chromatin Features

Figure S4

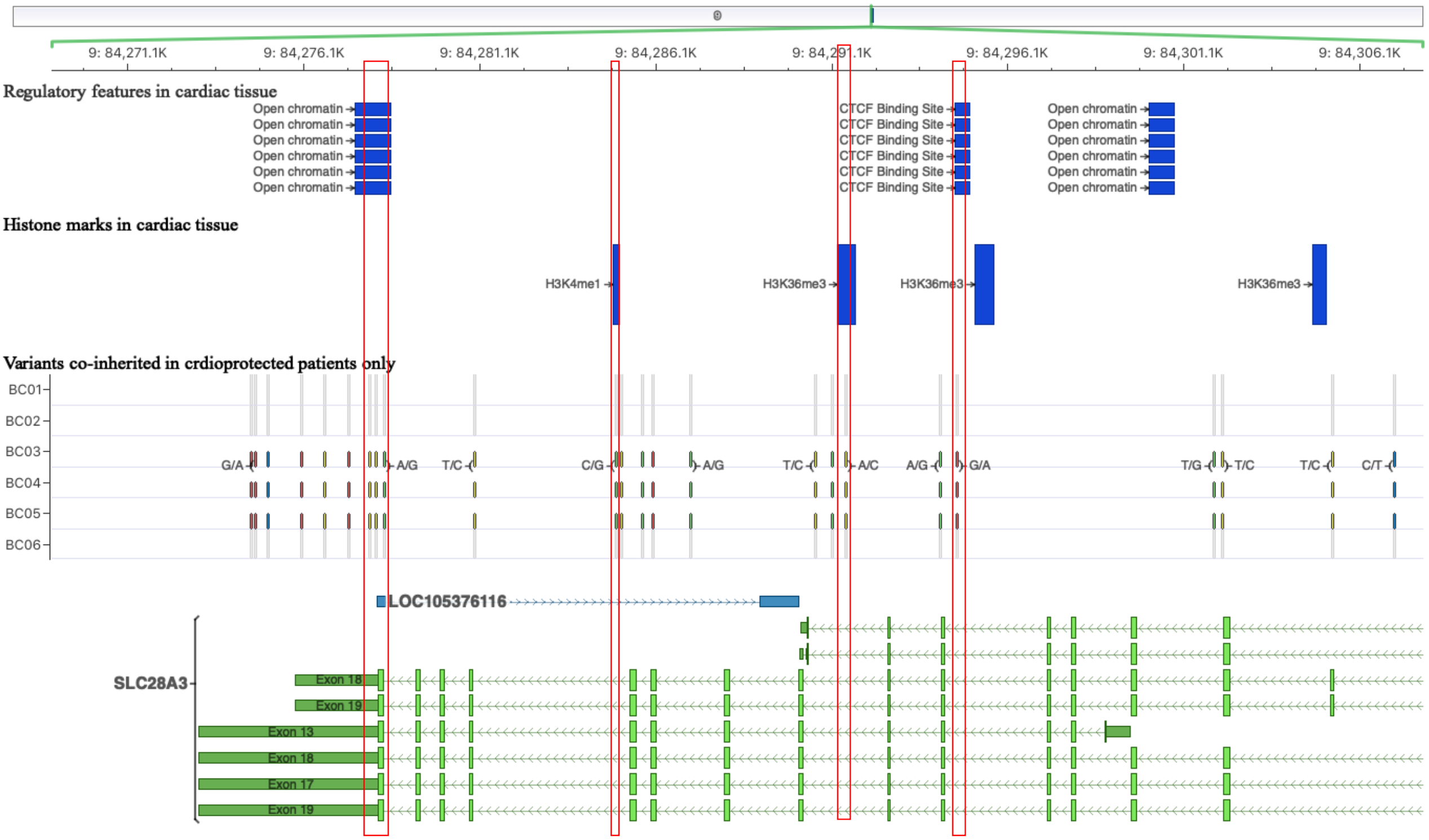
9
9: 84,271.1K
9: 84,276.1K
9: 84,281.1K
9: 84,286.1K
9: 84,291.1K
9: 84,296.1K
9: 84,301.1K
9: 84,306.1K
Regulatory features in cardiac tissue
Open chromatin
CTCF Binding Site
Histone marks in cardiac tissue
H3K4me1
H3K36me3
Variants co-inherited in crdioprotected patients only
BC01
BC02
BC03
BC04
BC05
BC06
G/A
A/G
T/C
C/G
A/C
T/G
C/T
LOC105376116
SLC28A3
Exon 18
Exon 19
Exon 13
Exon 17

Figure S5

Supplementary Figures legends

Figure S1. Generation of *SLC28A3* amplicons, related to Figure 1. (A) Exemplary agarose gel picture for all nine overlapping *SLC28A3* amplicons generated from one sample. L, ladder; 1-9, amplicons one to nine. **(B)** Exemplary pre-nanopore sequencing amplicon validation by sanger sequencing for amplicon number four (Amp04). Top panel shows the first ~ 600 bp of generated amplicon four (AMP04) aligned to its reference sequence (AMP04 ref). Bottom panel shows a zoom-in view for the first ~ 100 bp of generated amplicon four perfectly matching its reference sequence.

Figure S2. Cumulative yield of demultiplexed sequence reads, related to Figure 1. (A) Cumulative sequence yield in gigabase (GB) generated over 48 h. **(B)** Cumulative number of sequence reads generated over 48 h.

Figure S3. Alignment of Nanopore sequence reads, related to Figure 1. Dot plot showing reads percentage identity versus reads average base quality for each study sample. Histogram on the x-axis shows number of reads with relevant percentage identity. Histogram on the y-axis shows number of reads with relevant average base quality.

Figure S4. Effect of candidate SNPs on chromatin features binding sites, related to Figure 3. Effect of each SNP on altering chromatin features (transcription factors, DNase hypersensitive site, and histone marks) binding sites. Log2 fold change measure the fold change in the probability of observing a binding site for relevant chromatin feature between reference and alternative allele for a particular SNP**.**

Figure S5. Candidate SNPs located at regulatory regions in human cardiac tissue, related to Figure 3. Regulatory regions assessed included transcription factors, histone mark, and DNase hypersensitive regions in human cardiac tissue integrated in ensemble regulatory build. SNPs marked by red rectangles are SNPs that are located in regulatory regions binding sites.

Table S1. Inclusion and exclusion criteria, related to Figure 1.

Inclusion Criteria	Exclusion Criteria
Diagnosis of cancer	Unwilling to consent/assent to ≤10 ml blood draw
Treatment with doxorubicin (Adriamycin)	
Age ≤18 years at time treatment	
Documentation of pre–chemotherapy shortening fraction of ≥30%	No documentation of pre-chemotherapy echocardiography shortening fraction
For affected patients only: SF of ≤24% or signs and symptoms of cardiac compromise requiring intervention based on CTCAEv3. Only echos ≥ 21 d after doxorubicin dose are to be considered.	
For control patients: SF of ≥24% and no symptoms of cardiac compromise for at least 5 years after treatment	

Table S2. Doxorubicin–treated patients recruited in this study, related to Figure 1.

ID	Anthracycline	Cardiotoxicity	Gender	Age at Treatment	Cancer diagnosis	Heart radiation	rs7853758
BC01	Yes	Yes	Male	5.1	Wilm's Tumor	Yes	GG
BC02	Yes	Yes	Male	1.6	ALL	No	GG
BC06	Yes	Yes	Female	4.3	ALL	No	GG
BC03	Yes	No	Female	2.7	ALL	No	AG
BC04	Yes	No	Female	2.2	ALL	No	AG
BC05	Yes	No	Male	1.6	ALL	No	AG

Radiation therapy includes significant radiation exposure to the heart or surrounding tissue. This includes mantle and mediastinal radiation, whole–lung radiation, whole–abdomen or upper abdominal radiation, left–side flank radiation and total–body irradiation. SF, shortening fraction; NA, not applicable

Table S3: primers for *SLC28A3* amplicons amplification, related to Figure 1.

Primer ID	Sequence 5'>3'	Direction	Amplicon length (bp)
Amp01_fw	AGTTGCATGTTGCCATTCTG	Forward	9218
Amp01_rw	GTTGCTGTAGCCCTCAGCTC	Reverse	
Amp02_fw	CTCCCCAGGAGTGCAAATAG	Forward	9908
Amp02_rv	TCAAGGGGAATCACTTCAGG	Reverse	
Amp03_fw	TCAAGTTTGCATGATCACACC	Forward	8979
Amp03_rv	CAGGAAATATGGCTTCAGCTC	Reverse	
Amp04_fw	AAGGAAGATCCCACGTTGTG	Forward	9286
Amp04_rv	AAGTGATGCTTCCCATCAGG	Reverse	
Amp05_fw	GCTGTTTGTTGAATCGGATG	Forward	9306
Amp05_rv	TCCAACTGTCTGAGCACCAG	Reverse	
Amp06_fw	TGTTGCAGGTGTTTGGAAAG	Forward	5732
Amp06_rv	ACATTATGAGCCCACCGAAG	Reverse	
Amp07_fw	CGGCCGCTGGTGAGGTCCCCCAA	Forward	8668
Amp07_rv	TGGGCAGTGGTGCTGGCAAGCGT	Reverse	
Amp08_fw	TTGGCAATGTCCGGATTC	Forward	9420
Amp08_rv	TTCCCCTTTCCAGGGATAAC	Reverse	
Amp09_fw	GGACCTCTTCTCCCTGGAAC	Forward	9509
Amp09_rv	AGACCCTAAGGCCTCTCCAG	Reverse	

Table S4: PCR reaction mixture and conditions, related to Figure 1.

Amplicon ID	Composition of reaction mixture	PCR condition
Amp01, Amp02, Amp04, Amp05, and Amp09	10 µl 5X PrimeSTAR GXL Buffer, 4 µl dNTP Mixture (2.5 mM each), 1 µl of 100 µM primer, 300 ng DNA template, and 1 µl PrimeSTAR GXL DNA Polymerase 1.25 U/50, and Sterile distilled water to 50 µl	30 cycles 98℃ 10 sec 60℃ 15 sec 68℃ 10 min Hold at 4 ℃
Amp03, and Amp08	10 µl 5X PrimeSTAR GXL Buffer, 4 µl dNTP Mixture (2.5 mM each), 1 µl of 100 µM primer, 300 ng DNA template, and 1 µl PrimeSTAR GXL DNA Polymerase 1.25 U/50, and Sterile distilled water to 50 µl	30 cycles 98℃ 10 sec 58℃ 15 sec 68℃ 10 min Hold at 4 ℃
Amp06	10 µl 5X PrimeSTAR GXL Buffer, 4 µl dNTP Mixture (2.5 mM each), 1 µl of 100 µM primer, 300 ng DNA template, and 1 µl PrimeSTAR GXL DNA Polymerase 1.25 U/50, and Sterile distilled water to 50 µl	30 cycles 98℃ 10 sec 60℃ 15 sec 68℃ 6 min Hold at 4 ℃
Amp07	10 µl 5X PrimeSTAR GXL Buffer, 4 µl dNTP Mixture (2.5 mM each), 1 µl of 100 µM primer, 300 ng DNA template, and 1 µl PrimeSTAR GXL DNA Polymerase 1.25 U/50, and Sterile distilled water to 50 µl	30 cycles 98℃ 10 sec 66℃ 15 sec 68℃ 6 min Hold at 4 ℃

Table S5: Quality assessment of *SLC28A3* amplicons, related to Figure 1.

Sample ID	Amplicon	Conc (ng/µl)	A260	A280	260/280	260/230
BC01	Amp01	117.2	2.344	1.232	1.9	1.72
	Amp02	7.525	0.15	0.095	1.58	1.69
	Amp03	74.43	1.489	0.771	1.93	1.73
	Amp04	48.37	0.967	0.514	1.88	2.08
	Amp05	128.3	2.566	1.342	1.91	1.94
	Amp06	59.79	1.196	0.649	1.84	1.62
	Amp07	90.3	1.806	0.971	1.86	1.69
	Amp08	7.217	0.144	0.074	1.95	1.52
	Amp09	146.8	2.936	1.546	1.9	2.13
BC02	Amp01	148.3	2.967	1.57	1.89	2.14
	Amp02	80.62	1.612	0.88	1.83	1.72
	Amp03	51.97	1.039	0.549	1.89	1.75
	Amp04	107.7	2.154	1.142	1.89	1.96
	Amp05	98.96	1.979	1.06	1.87	1.95
	Amp06	122.6	2.453	1.288	1.9	1.94
	Amp07	103.4	2.069	1.123	1.84	1.88
	Amp08	19.44	0.389	0.217	1.79	2.04
	Amp09	81.35	1.627	0.855	1.9	2.02
BC06	Amp01	96.78	1.936	1.016	1.91	2.09
	Amp02	60.44	1.209	0.672	1.8	1.57
	Amp03	73.76	1.475	0.796	1.85	1.72
	Amp04	134.1	2.681	1.424	1.88	2.07
	Amp05	84.22	1.684	0.887	1.9	1.92
	Amp06	41.24	0.825	0.439	1.88	1.86
	Amp07	104.5	2.089	1.095	1.91	2.11
	Amp08	45.57	0.911	0.496	1.84	1.79
	Amp09	73.19	1.464	0.81	1.81	1.67
BC03	Amp01	120.1	2.403	1.284	1.87	2.07
	Amp02	40.18	0.804	0.449	1.79	1.61
	Amp03	58.98	1.18	0.631	1.87	1.8
	Amp04	91.2	1.824	0.973	1.87	1.92
	Amp05	114.6	2.293	1.241	1.85	1.72
	Amp06	93.09	1.862	0.979	1.9	2.01
	Amp07	106.4	2.128	1.11	1.92	1.77
	Amp08	64.44	1.289	0.711	1.81	1.91
	Amp09	61.63	1.233	0.651	1.89	2.08
BC04	Amp01	147	2.94	1.551	1.9	1.79
	Amp02	38.41	0.768	0.405	1.9	1.78
	Amp03	35.4	0.708	0.387	1.83	1.56
	Amp04	155.2	3.105	1.664	1.87	1.91
	Amp05	101.4	2.028	1.045	1.94	1.98
	Amp06	46.66	0.933	0.494	1.89	1.88
	Amp07	82.67	1.653	0.911	1.81	1.9
	Amp08	14.07	0.281	0.15	1.88	1.81
	Amp09	61.4	1.228	0.663	1.85	2.11
BC05	Amp01	72.96	1.459	0.771	1.89	1.72
	Amp02	116.3	2.327	1.246	1.87	2.13

	Amp03	125.4	2.509	1.312	1.91	2.2
	Amp04	59.99	1.2	0.644	1.86	1.55
	Amp05	33.31	0.666	0.353	1.89	1.79
	Amp06	141.3	2.826	1.515	1.87	1.73
	Amp07	27.08	0.542	0.295	1.84	1.59
	Amp08	41.91	0.838	0.44	1.91	1.72
	Amp09	90.51	1.81	0.978	1.85	1.83

Table S7: Genotype concordance between Nanopore sequencing and genotyping on InfiniumOmniExpress-24v1-2, related to Figure 2.

Type	Count	Percent of total
REF/REF	421	74.78
REF/ALT1	0	0.00
REF/ALT2	0	0.00
ALT1/REF	46	8.17
ALT1/ALT1	74	13.14
ALT1/ALT2	0	0.00
ALT2/REF	3	0.53
ALT2/ALT1	0	0.00
ALT2/ALT2	19	3.37
Total	563	100.00

The genotypes are: homozygous reference (REF), heterozygous (ALT1), and homozygous non-reference (ALT2). The pairs of genotypes, e.g., REF/REF, on each row represent genotype calls by nanopore sequence and by the Omni chip respectively. REF/REF, ALT1/ALT1, and ALT2/ALT2 indicate concordant genotypes. Line graph represents genotype percentage of total

Table S8: Regulatory properties of *SLC28A3* SNPs coinherited only in cardio protected patients, related to Figure 3.

rs ID	No. of altered chromatin feature binding sites
rs11140490	206
rs4877835	204
rs4877836	141
rs7867504	134
rs4877272	107
rs885004	105
rs12237803	52
rs3750406	41
rs12003403	40
rs10868135	33
rs4877831	32
rs4877833	31
rs10868137	30
rs7853758	11
rs7858075	6
rs7047315	4
rs7853066	4
rs7030019	3
rs12003423	2
rs7047898	2
rs11140488	1
rs4877834	1

Table S9: *SLC28A3* SNPs coinherited only in cardio protected patient affecting chromatin feature binding sites (showing only SNPs with Log2 fold change value >=1), related to Figure 3.

rs ID	Cell type| chromatin| treatment	E-value	Log2 fold change
rs4877272	ECC-1|ERalpha|BPA_100nM	0.01	-1.01
	H1-hESC|TEAD4|None	0.01	-1.60
	NT2-D1|DNase|None	0.03	-1.22
	NHEK|DNase|None	0.03	-1.01
	H7-hESC|DNase|None	0.03	-1.22
	H1-hESC|DNase|None	0.04	-1.22
	RWPE1|DNase|None	0.05	-1.09
rs7867504	GM12878|JunD|None	0.00	-1.11
	PrEC|DNase|None	0.01	-1.55
	GM12878|BATF|None	0.01	-1.34
	GM12865|DNase|None	0.01	-1.04
	GM12864|DNase|None	0.01	-1.00
	SAEC|DNase|None	0.01	-1.62
	HMEC|DNase|None	0.01	-1.12
	HEEpiC|DNase|None	0.01	-1.52
	pHTE|DNase|None	0.01	-1.06
	NHEK|DNase|None	0.01	-1.17
	HRCEpiC|DNase|None	0.02	-1.18
	HRE|DNase|None	0.02	-1.21
	HPDE6-E6E7|DNase|None	0.02	-1.22
	MCF10A-Er-Src|STAT3|4OHTAM_1uM_12hr	0.02	-1.30
	MCF10A-Er-Src|STAT3|EtOH_0.01pct_12hr	0.02	-1.25
	MCF10A-Er-Src|c-Fos|4OHTAM_1uM_12hr	0.02	-1.81
	MCF10A-Er-Src|c-Myc|4OHTAM_1uM_4hr	0.02	-1.06
	MCF10A-Er-Src|STAT3|EtOH_0.01pct_4hr	0.02	-1.18
	MCF10A-Er-Src|STAT3|4OHTAM_1uM_36hr	0.02	-1.21
	MCF10A-Er-Src|STAT3|EtOH_0.01pct	0.02	-1.00

	MCF10A-Er-Src|c-Fos|4OHTAM_1uM_4hr	0.02	-1.67
	RWPE1|DNase|None	0.02	-1.17
	HUVEC|c-Fos|None	0.03	-1.09
	MCF10A-Er-Src|c-Fos|EtOH_0.01pct	0.03	-1.66
	MCF10A-Er-Src|c-Fos|4OHTAM_1uM_36hr	0.03	-1.82
	HMVEC-dBl-Ad|DNase|None	0.03	-1.13
	RPTEC|DNase|None	0.03	-1.01
	HMVEC-dLy-Neo|DNase|None	0.03	-1.02
	WI-38|DNase|4OHTAM_20nM_72hr	0.04	-1.28
	HMVEC-LBl|DNase|None	0.04	-1.18
	HUVEC|c-Jun|None	0.04	-1.01
	HFF-Myc|DNase|None	0.05	-1.03
	NHLF|DNase|None	0.05	-1.16
rs11140490	Melano|DNase|None	0.00	1.05
	HSMM_emb|DNase|None	0.00	1.22
	HSMMtube|DNase|None	0.00	1.42
	NHDF-neo|DNase|None	0.00	1.76
	NHDF-Ad|DNase|None	0.00	1.73
	AG10803|DNase|None	0.00	1.56
	ProgFib|DNase|None	0.00	1.34
	FibroP|DNase|None	0.00	1.25
	HGF|DNase|None	0.00	1.56
	HPdLF|DNase|None	0.00	1.58
	Stellate|DNase|None	0.00	1.36
	HCF|DNase|None	0.00	1.42
	AG09319|DNase|None	0.00	1.46
	HSMM|DNase|None	0.00	1.36
	SK-N-SH|TAF1|None	0.00	1.07
	HFF|DNase|None	0.00	1.35
	BJ|DNase|None	0.00	1.42
	HCM|DNase|None	0.00	1.42

	AG09309|DNase|None	0.00	1.45
	Myometr|DNase|None	0.00	1.16
	AG04449|DNase|None	0.00	1.37
	HPF|DNase|None	0.00	1.51
	AoAF|DNase|None	0.00	1.36
	AoSMC|DNase|None	0.00	1.40
	SKMC|DNase|None	0.00	1.29
	PanIsletD|DNase|None	0.00	1.18
	HMF|DNase|None	0.00	1.42
	HPAF|DNase|None	0.00	1.31
	HConF|DNase|None	0.00	1.37
	HAc|DNase|None	0.00	1.07
	HFF-Myc|DNase|None	0.00	1.08
	HBMEC|DNase|None	0.00	1.29
	WI-38|DNase|4OHTAM_20nM_72hr	0.00	1.17
	NH-A|DNase|None	0.01	1.16
	WI-38|DNase|None	0.01	1.25
	NHLF|DNase|None	0.01	1.15
	AG04450|DNase|None	0.01	1.21
	HCFaa|DNase|None	0.01	1.13
	HNPCEpiC|DNase|None	0.01	1.16
	HVMF|DNase|None	0.01	1.26
	HCPEpiC|DNase|None	0.01	1.05
	HIPEpiC|DNase|None	0.01	1.06
	HAEpiC|DNase|None	0.01	1.10
rs4877835	NHDF-Ad|DNase|None	0.01	1.07
	NHDF-neo|DNase|None	0.01	1.06
	BE2_C|DNase|None	0.01	1.08
	SK-N-SH_RA|DNase|None	0.01	1.08
rs10868137	H1-hESC|TCF12|None	0.00	1.07
	GM12878|ZEB1|None	0.00	1.06

E-value, expect value stands for the significance of each individual chromatin feature predicted score; Log2 fold change, measure the fold change in the probability of observing a binding site for relevant chromatin feature between reference and alternative allele for a particular SNP (Zhou and Troyanskaya, 2015).

Table S10: *SLC28A3* SNPs coinherited only in cardio protected patient located at regulatory regions and histone marks in cardiac tissues, and at transcription factor binding sites using ensemble regulatory build, related to Figure 3.

SNPs	Position	Histone marks in cardiac tissue	Regulatory region in cardiac tissue	Motifs present at SNP locus
rs3750406	84277979	—	Open chromatin	TEAD4::RFX5, FOXJ3::TBX21, SOX6::TBX21, ELK1::FOXI1, ETV2::FOXI1, MGA, TBX2, TBX4, TBX5, ONECUT1, ONECUT2, ONECUT3, HOXB2::EOMES,HOXB2::TBX21, HOXB2::TBX3, MGA::DLX2, MGA::DLX3, MGA::EVX1, PITX1::HES7, E2F3::ONECUT2,TFAP2C::ONECUT2, ETV2::SREBF2, CUX1::SOX15, HOXB13::EOMES, HOXB13::TBX21,HOXD12::TBX21, TBX20, KLF13, KLF14,SREBF2, GLIS1, EOMES, SNAI2, TCF3, TCF4, THRB (n=36)
rs7858075	84278156	—	Open chromatin	TEAD4::FOXI1, IRF3, ETV2::SOX15, POU2F1::FOXO6, POU2F1::DLX2, TEAD4::FOXI1 (n=6)
rs11140490	84278398	—	Open chromatin	CLOCK::FIGLA, TEAD4::EOMES, TEAD4::TBX21, ETV2::DRGX, ZIC1, ZIC3, ZIC4, HOXB2::NHLH1,TEAD4::TCF3, GCM2::SOX15, and TEAD4::FIGLA (n=11)
rs4877831	84284969	H3K4me1	—	—
rs7047898	84291502	H3K36me3	—	—
rs10868137	84294167	—		TFAP2C::DLX3, FOXO1::HOXB13, MGA::DLX3, HOXB2::TCF3 (n=4)
rs885004	84294635	—	CTCF binding site	THRB, TEAD4::CEBPD, ERF::PITX1, ETV2::GSC2, ERF::ONECUT2, ETV2::ONECUT2, FLI1::ONECUT2, POU2F1::DLX2, R, X3::SRF, TEAD4::PAX5, PITX1::HES7, HESX1, LHX9, HOXD12::HOXA3, ZBED1, BARHL2, E2F1, E2F2, E2F3, BARX1, MSX1, MSX2, TBX1, TBX20, HOXB13::EOMES, HOXB13::TBX21, TEAD4::HOXB13, PBX4::HOXA1, PBX4::HOXA10, ONECUT1, ONECUT2, HMX1, HMX2, HMX3, CUX1::SOX15, TFAP2C::ONECUT2 (n=36)
rs4877835	84301936	—		POU2F1::FOXO6, POU2F1::EOMES, CLOCK::BHLHA15, MAX, TFAP4::MAX, HOXD12::EOMES, FOXO1, FOXO3, FOXO4, FOXO6, CTCF, ZNF238, ASCL2, BHLHA15, BHLHE22, BHLHE23,MESP2, MSC, MYF6, NEUROD2, NEUROG2, NHLH1, OLIG1, OLIG2, OLIG3, TCF15, TFAP4, ESRRA, ESRRG, FOXJ2::HOXB13 (n=30)
rs4877836	84302173	—		MYBL1, MYBL2, IRF4, IRF5, IRF8, IRF9, ELK1::FOXI1, ERF::FOXI1, ETV2::FOXI1, ETV5::FOXI1, FLI1::FOXI1, FOXO1::ELF1, FOXO1::ELK1, ELK1::HOXA3 (n=14)

Table S11: eQTL (expression quantitative trait loci) functional annotation of *SLC28A3* SNPs coinherited only in cardio protected patients, related to Figure 3.

SNP Id	*P*-value	NES	Tissue
rs10868133	2.10E-07	-0.22	Cells - Cultured fibroblasts
	4.50E-07	0.21	Thyroid
rs10868135	4.10E-07	-0.22	Cells - Cultured fibroblasts
	0.0000034	0.2	Thyroid
rs10868137	3.80E-07	0.23	Thyroid
	6.70E-07	-0.22	Cells - Cultured fibroblasts
rs11140488	1.60E-07	-0.22	Cells - Cultured fibroblasts
	2.60E-07	0.22	Thyroid
rs11140489	1.50E-07	-0.22	Cells - Cultured fibroblasts
	4.20E-07	0.21	Thyroid
rs11140490	1.40E-07	-0.22	Cells - Cultured fibroblasts
	6.30E-07	0.21	Thyroid
rs12003403	1.60E-07	-0.22	Cells - Cultured fibroblasts
	2.60E-07	0.22	Thyroid
rs12003423	1.60E-07	-0.22	Cells - Cultured fibroblasts
	7.20E-07	0.21	Thyroid
rs12237803	4.70E-08	-0.24	Cells - Cultured fibroblasts
	7.50E-08	0.24	Thyroid
rs3750406	1.40E-07	-0.22	Cells - Cultured fibroblasts
	6.30E-07	0.21	Thyroid
rs4877272	6.40E-08	-0.23	Cells - Cultured fibroblasts
	5.60E-07	0.21	Thyroid
rs4877831	6.00E-09	-0.21	Cells - Cultured fibroblasts
	0.000021	0.16	Thyroid
rs4877833	5.30E-07	-0.21	Cells - Cultured fibroblasts
	8.90E-07	0.21	Thyroid
rs4877834	4.70E-08	0.24	Thyroid
	7.40E-07	-0.21	Cells - Cultured fibroblasts
rs4877835	4.20E-07	0.23	Thyroid
	5.20E-07	-0.22	Cells - Cultured fibroblasts
rs4877836	3.10E-07	-0.23	Cells - Cultured fibroblasts
	3.30E-07	0.23	Thyroid
rs7030019	1.70E-08	0.25	Thyroid
	8.70E-08	-0.23	Cells - Cultured fibroblasts
	0.000014	0.64	Brain - Amygdala

rs7047315	3.80E-07	0.23	Thyroid
	6.70E-07	-0.22	Cells - Cultured fibroblasts
rs7047898	3.80E-07	0.23	Thyroid
	6.70E-07	-0.22	Cells - Cultured fibroblasts
rs7853066	1.50E-07	0.23	Thyroid
	7.00E-07	-0.21	Cells - Cultured fibroblasts
rs7853758	3.10E-08	0.23	Thyroid
	0.0000019	-0.2	Cells - Cultured fibroblasts
	0.000014	0.61	Brain - Amygdala
rs7867504	0.000003	-0.16	Cells - Cultured fibroblasts
rs885004	1.30E-07	-0.23	Cells - Cultured fibroblasts
	1.90E-07	0.23	Thyroid

NES, normalized effect size; This analysis was done using GTEX eQTL database

Table S12: Quality Control of Genotype Imputation, related to Figure 4.

Posterior probability intervals	Number of Genotypes	% Concordance	Posterior probability intervals	% Called	% Concordance
[0.0-0.1]	0	0	[>= 0.0]	100	95.7
[0.1-0.2]	0	0	[>= 0.1]	100	95.7
[0.2-0.3]	0	0	[>= 0.2]	100	95.7
[0.3-0.4]	0	0	[>= 0.3]	100	95.7
[0.4-0.5]	1	0	[>= 0.4]	100	95.7
[0.5-0.6]	0	0	[>= 0.5]	99.8	96.4
[0.6-0.7]	0	0	[>= 0.6]	99.8	96.4
[0.7-0.8]	3	0	[>= 0.7]	99.8	96.4
[0.8-0.9]	4	100	[>= 0.8]	99.8	97.8
[0.9-1.0]	130	100	[>= 0.9]	99.5	98.5

Table S14: Cost estimates of Nanopore candidate loci sequencing compared to Illumina targeted sequencing, , related to Figure 4.

Steps	**Cost per ~100kb / sample in USD**							
	Nanopore MinION Sequencing				**Illumina Targeted Sequencing**			
Number of multiplexed samples	*n* = 6	*n* = 12	*n* = 24	*n* = 96	*n* = 6	*n* = 12	*n* = 24	*n* = 96
Library preparation	16.6[a]	8.33[a]	4.16[a]	1.04[a]	35.83[b]	35.83[b]	35.83[b]	35.83[b]
Samples barcoding	4[c]	4[c]	4[c]	1.77[c]	7[d]	7[d]	7[d]	7[d]
Sequencing	5.20[e]	5.20[e]	5.20[e]	5.20[e]	160[f]	80[f]	40[f]	10[f]
Total cost	**25.8**	**17.54**	**13.37**	**8.02**	**313.67**	**178.25**	**110.54**	**57.99**

[a]Library preparation using SQK-LSK109 kit. [b]Library preparation using Nextera XT DNA Library Preparation Kit. [c] Sample barcoding using EXP-NBD104 or EXP-NBD 114 or EXP-PBC096 kits. [d] Sample barcoding using Illumina Nextera DNA Unique Indexes. [e]Sequencing using Nanopore MinION (1 flow cell). Unlike Miseq, real-time data analysis provides the privilege of controlling the utilization of the Minion flow cell. Once sufficient coverage is reached, the sequencing is stopped, flow cell is washed and stored until the next experiment. [f]Sequencing using Miseq 600-cycle (one flow cell). The cost of the devices and kits are adopted from https://nanoporetech.com/products/comparison and https://www.illumina.com/products.html

Transparent Methods

Patient recruitment and hiPSC-CM generation.

SNP rs7853758 is associated with cardioprotective effect after doxorubicin treatment in a Canadian pediatric patient population, and has been validated in both Dutch and US patient populations (Aminkeng et al., 2015). With written consent, six well–phenotyped, doxorubicin–exposed patients from the Canadian cohort were specifically re–recruited according to the original inclusion criteria (**Table S1 and S2**). This study was approved by the individual ethics committees or institutional review boards of the universities and institutions where patients were enrolled. Written informed consent or assent was obtained from patients or their parents or legal guardians in accordance with the Declaration of Helsinki as revised in 2008. Peripheral blood was drawn from three pediatric patients who carried a heterozygous SNP and were protected from doxorubicin-induced cardiotoxicity (BC03, BC04, and BC05), and three control patients who did not carry this protective SNP and developed cardiotoxicity upon same doxorubicin therapy (BC01, BC02, and BC06). Detailed patient demographics and phenotype, including age, sex, ethnicity, type of cancer, treatment regime and cardiovascular function, are all well documented (Visscher et al., 2012, Visscher et al., 2013). Genomically stable hiPSC lines from each individual have been established after non-integrating (Sendai virus-based) reprogramming (Burridge et al., 2016, Burridge et al., 2015).

DNA extraction and purification.

DNA was isolated from six patients derived human induced pluripotent stem cells, using QuickExtract DNA Extraction Solution (Epicenter) according to manufacturer protocol. Isolated DNA was then purified using Genomic DNA Clean & Concentrator-10 (Zymo research) according to manufacturer protocol.

SLC28A3 locus amplification and amplicons validation.

About 75 kb located on chr9: 84,274,029-84,349,802 (NC_000009.12, GRCh38.p7) encompassing the coding region of *SLC28A3* gene (chr9: 84,340,634-84,278,218) plus 9 kb and 5 kb at the 5'UTR and 3`UTR, respectively were amplified using long range PCR. A set of primer pairs were designed to amplify nine overlapping amplicons covering the target region whereas, the

length of amplicons ranged between 5732 and 9908 bp (**Table S3**). Generation of overlapping amplicons help compensate for the low depth of coverage at the start and the end of each sequence read. Using ~200 ng of DNA per reaction, amplicons were amplified using PrimeSTAR GXL DNA Polymerase (Takara) via three steps-PCR. PCR conditions were optimized for each amplicon to avoid any unspecific amplification. PCR reaction mixture components and cycling conditions are mentioned in **Table S4.** Amplified amplicons were then purified using PureLink PCR Purification Combo Kit (Thermo Scientific) to get rid of contaminants that could damage the pores of the Nanopore flow cell, and eventually decrease the number of the sequencing reads.

Amplicon validation prior sequencing

PCR products (amplicons) were run on 1% agarose gel and visualized by staining with GelGreen Nucleic Acid Stain (Biotium) (**Figure S1A**). Gel bands corresponding to target amplicons size were confirmed for all amplified amplicons. For further confirmation, ~ 1 kb at the start and the end of each purified amplicon were then Sanger sequenced, and *in silico* aligned to its relevant reference sequence (**Figure S1B**). The quality and concentration of the generated amplicons were assessed using NanoDrop 8000 and Qubit 3.0 fluorometer, respectively **(Table S5)**. It is important to generate amplicons with reasonable purity to avoid ruining the pores of the flow cell which decreases the number of generated sequence reads. Thus, amplicons with 260/280 and 260/230 absorbance ratios of less than 1.8 and 1.5, respectively were excluded and regenerated.

MinION library preparation and flow cell loading

Library preparation was done using ligation sequencing (Oxford, Nanopore, SQK-LSK108) and 1D Native barcoding (Oxford, Nanopore, EXP-NBD103) kits. All amplicons were pooled together in an equimolar amount and repaired using NEBNext End repair / dA-tailing Module (New England Biolabs, E7546). Reaction mix was prepared by adding 45 µl eluted DNA to 7 µl Ultra II End-prep reaction buffer, 10 µl Ultra II End-prep enzyme mix, and 5 µl nuclease-free water. Reaction mix was then incubated for 5 min at 20 °C followed by 5 min at 65 °C. DNA was then purified using AMPure XP beads (see above). Finally, 25 µl clear elute was transferred into DNA LoBind tube.

Each sample was then barcoded using 1D Native barcoding (Oxford, Nanopore, EXP-NBD103), by adding 2.5 µl native Barcode to 22.5 µl end-prepped DNA, and 25 µl Blunt/TA

Ligase Master Mix (New England Biolabs, M0367). Reaction mix was then incubated for 10 min at room temperature, DNA was then purified using AMPure XP beads (see above), and 26 µl of clear elute was transferred into Eppendorf DNA LoBind tube.

Barcoded samples were pooled in an equimolar amount to a final concentration of 700 ng, then diluted by adding 24 µl nuclease free water. Adapters were then ligated using NEBNext Quick Ligation Module (New England Biolabs, E6056). Pooled DNA (700 ng) was then mixed with 20 µl Barcode Adapter Mix, 20 µl NEBNext Quick Ligation Reaction Buffer, and 10 µl Quick T4 DNA Ligase. Reaction mix was then incubated for 10 min at room temperature, and DNA was then purified by adding 62 µl AMPure XP beads Beckman Coulter, A63880), incubated on a hula mixer at room temperature for 5 min, spun down, and pelleted on a magnet, and supernatant was discarded. Beads were then resuspended in 140 µl Adapter Bead Buffer (ABB) by flicking the tube, pelleted on magnet, and supernatant was discarded (resuspension step was repeated). Pellet was resuspended in 15 µl Elution Buffer, incubated for 10 min at room temperature, pelleted on magnet until the elute is clear, and finally 15 µl clear elute was transferred into Eppendorf DNA LoBind tube.

Priming mix was prepared by adding 576 µl RBF to 624 µl nuclease-free water, then 800 µl priming mix was loaded on the flow cell using priming port dropwise to avoid the introduction of air bubbles. Five minutes later, SpotON sample cover on MinION was opened and 200 µl priming mix was loaded. DNA library was prepared for loading by adding 12 µl DNA library to 35 µl RBF, 25.5 µl LLB, and 2.5 µl nuclease-free water. DNA library was gently mixed, loaded on the flow cell (FLO-MIN 106 R9 version, FAF19356) through SpotON port. Library was then sequenced for 48 hours with live base-calling.

Raw sequencing data and SNPs functional analysis

Raw barcoded sequence reads were demultiplexed into six fastaq files using Porechop (Wylie et al., 1996). Quality of demultiplexed sequence reads were assessed using Nanopack (De Coster et al., 2018). Sequence reads were then aligned to reference human genome (GRCh38.p92) using minimap2 (Li, 2018) "-ax map-ont", sam files were then sorted and converted into bam files using SAMtools (Li et al., 2009). Bam files were down-sampled using SAMtools "-s 0.1 to -s 0.9", and the quality of aligned reads were assessed using Nanopack (De Coster et al., 2018). Depth of

coverage analysis was done using deepTools2 (Ramirez et al., 2016). Sequence reads were indexed and variants were called using Nanopolish (Loman et al., 2015). Variant call format files containing called SNPs were processed and analyzed using several tools including VCFtools (Danecek et al., 2011), SnpSift (Cingolani et al., 2012), and BCFtools (Narasimhan et al., 2016). SNPs functional annotation analysis was done using DeepSEA (Zhou and Troyanskaya, 2015), R (RCoreTeam) and BiomaRt (Durinck et al., 2009) Bioconductor package that includes multiple ensemble gene regulation database. Conservation analysis was done using SnpSift (Cingolani et al., 2012) and PhastCons dataset that includes genome-wide multiple alignments with other 99 vertebrate species. (http://hgdownload.cse.ucsc.edu/goldenpath/hg38/phastCons100way)

Genotype imputation analysis

First the vcf file containing the original GWAS dataset (23 genotypes in six samples) (Visscher et al., 2012) was converted to plink bed format that is compatible with the downstream analysis in SHAPEIT, using Plink " --make-bed " (Purcell et al., 2007). We then checked the alignment of SNPs between the GWAS dataset and the1000 genomes phase I reference panel using SHAPEIT "shapeit -check" (Delaneau et al., 2011). GWAS genotypes were then phased using SHAPEIT using 1000 genomes phase I haplotype reference panel. Additional SNPs that are not present on the GWAS genotyping platform were then imputed using the pre-phased GWAS genotypes with 1000 genomes phase I haplotype reference panel using " impute2 use_prephased_g -known_haps_g " in IMPUTE2 (Howie et al., 2009).

Supplementary References

Aminkeng, F., et al. 2015. A coding variant in RARG confers susceptibility to anthracycline-induced cardiotoxicity in childhood cancer. *Nat Genet,* 47**,** 1079-84.

Burridge, P. W., Diecke, S., Matsa, E., Sharma, A., Wu, H. & Wu, J. C. 2016. Modeling Cardiovascular Diseases with Patient-Specific Human Pluripotent Stem Cell-Derived Cardiomyocytes. *Methods Mol Biol,* 1353**,** 119-30.

Burridge, P. W., Holmstrom, A. & Wu, J. C. 2015. Chemically Defined Culture and Cardiomyocyte Differentiation of Human Pluripotent Stem Cells. *Curr Protoc Hum Genet,* 87**,** 21 3 1-15.

Cingolani, P., Patel, V. M., Coon, M., Nguyen, T., Land, S. J., Ruden, D. M. & Lu, X. 2012. Using Drosophila melanogaster as a Model for Genotoxic Chemical Mutational Studies with a New Program, SnpSift. *Front Genet,* 3**,** 35.

Danecek, P., et al. 2011. The variant call format and VCFtools. *Bioinformatics,* 27**,** 2156-8.

De Coster, W., D'hert, S., Schultz, D. T., Cruts, M. & Van Broeckhoven, C. 2018. NanoPack: visualizing and processing long-read sequencing data. *Bioinformatics,* 34**,** 2666-2669.

Delaneau, O., Marchini, J. & Zagury, J. F. 2011. A linear complexity phasing method for thousands of genomes. *Nat Methods,* 9**,** 179-81.

Durinck, S., Spellman, P. T., Birney, E. & Huber, W. 2009. Mapping identifiers for the integration of genomic datasets with the R/Bioconductor package biomaRt. *Nature Protocols,* 4**,** 1184-1191.

Howie, B. N., Donnelly, P. & Marchini, J. 2009. A flexible and accurate genotype imputation method for the next generation of genome-wide association studies. *PLoS Genet,* 5**,** e1000529.

Li, H. 2018. Minimap2: pairwise alignment for nucleotide sequences. *Bioinformatics,* 34**,** 3094-3100.

Li, H., Handsaker, B., Wysoker, A., Fennell, T., Ruan, J., Homer, N., Marth, G., Abecasis, G., Durbin, R. & Genome Project Data Processing, S. 2009. The Sequence Alignment/Map format and SAMtools. *Bioinformatics,* 25**,** 2078-9.

Loman, N. J., Quick, J. & Simpson, J. T. 2015. A complete bacterial genome assembled de novo using only nanopore sequencing data. *Nat Methods,* 12**,** 733-5.

Narasimhan, V., Danecek, P., Scally, A., Xue, Y., Tyler-Smith, C. & Durbin, R. 2016. BCFtools/RoH: a hidden Markov model approach for detecting autozygosity from next-generation sequencing data. *Bioinformatics,* 32**,** 1749-51.

Purcell, S., et al. 2007. PLINK: a tool set for whole-genome association and population-based linkage analyses. *Am J Hum Genet,* 81**,** 559-75.

Ramirez, F., Ryan, D. P., Gruning, B., Bhardwaj, V., Kilpert, F., Richter, A. S., Heyne, S., Dundar, F. & Manke, T. 2016. deepTools2: a next generation web server for deep-sequencing data analysis. *Nucleic Acids Res,* 44**,** W160-5.

Rcoreteam R: A Language and Environment for Statistical Computing.

Visscher, H., et al. 2012. Pharmacogenomic prediction of anthracycline-induced cardiotoxicity in children. *Journal of Clinical Oncology: Official Journal of the American Society of Clinical Oncology,* 30**,** 1422-1428.

Visscher, H., et al. 2013. Validation of variants in SLC28A3 and UGT1A6 as genetic markers predictive of anthracycline-induced cardiotoxicity in children. *Pediatric Blood & Cancer,* 60**,** 1375-1381.

Wylie, C., Kofron, M., Payne, C., Anderson, R., Hosobuchi, M., Joseph, E. & Heasman, J. 1996. Maternal beta-catenin establishes a 'dorsal signal' in early Xenopus embryos. *Development,* 122**,** 2987-96.

Zhou, J. & Troyanskaya, O. G. 2015. Predicting effects of noncoding variants with deep learning-based sequence model. *Nat Methods,* 12**,** 931-4.